journal

J. Am. Ceram. Soc., 92 [5] 967–983 (2009)
DOI: 10.1111/j.1551-2916.2009.02990.x


# Negative Temperature Coefficient Resistance (NTCR) Ceramic Thermistors: An Industrial Perspective

Antonio Feteira†

EPCOS OHG, Electronic Components and Parts, 43 Siemmensstraβe, A-8530 Deutschlandsberg, Austria

**Monitoring and control of temperature is of paramount importance in every part of our daily life. Temperature sensors are ubiquitous not only in domestic and industrial activities but also in laboratory and medical procedures. An assortment of temperature sensors is commercially available for such purposes. They range from metallic thermocouples to resistive temperature detectors and semiconductive ceramics, showing a negative temperature coefficient of resistance (NTCR). NTCR ceramic sensors occupy a respected market position, because they afford the best sensitivity and accuracy at the lowest price. Despite the enormous commercial success of NTCR thermistors, this area of advanced functional ceramics has not been recently reviewed. Nearly 100 years elapsed between the first report of NTCR behavior and the fabrication of NTCR devices. The manufacture of the first NTCR ceramic thermistors was problematic, as often the devices suffered from poor stability and nonreproducibility. Before NTCR ceramics could be seriously considered for mass production of thermistors, it was necessary to devote a large amount of R&D effort to study the nature of their semiconductivity and understand the influence of impurities/dopants and heat treatments on their electrical characteristics, particularly in their time dependence resistivity (aging). Simultaneously, from a technological viewpoint it was important to develop methods enabling reliable and permanent electrical contacts, and design suitable housing for ceramics, in order to preserve their electrical properties under conditions of variable oxygen partial pressure and humidity. These topics are reviewed in this article from an industrial perspective. Examples of common applications of NTCR thermistors and future challenges are also outlined.**

## I. Introduction

Four main types of sensors are used for temperature sensing in domestic, industrial, and medical applications. Those are categorized as follows: (i) thermocouples, (ii) resistance temperature detectors (RTDs), (iii) integrated circuit (IC) sensors, and (iv) thermistors.‡ The capabilities, advantages, and disadvantages offered by each type of sensor are summarized in Table I. Obviously, the choice of a particular sensor depends on the required accuracy, speed of response, temperature range, thermal coupling, environment (chemical, electrical, or physical), and cost. Except for IC sensors, all the temperature sensors have nonlinear transfer functions, i.e. the temperature dependence of the physical parameter under scrutiny (e.g. resistance, voltage output, etc) is nonlinear.

Thermocouples are widely used as temperature sensors because they are small, robust, relatively inexpensive, easy to use, and cover the widest temperature range, as indicated in Table I. They are especially useful for making measurements at extremely high temperatures (up to +2300°C). Nonetheless, they must be shielded from harsh atmospheres and liquids due to corrosion degradation. The most common metals used for the fabrication of thermocouples are iron, platinum, rhenium, tungsten, copper, alumel (Al–Ni alloy), cromel (Ni–Cr alloy), and constantan (Cu–Ni alloy).[1] The output given by thermocouples is only in the range of a few millivolts; therefore they require precision amplification for further information processing. Nevertheless, their main disadvantages are associated with lower sensitivity (microvolts per degree) and accuracy in comparison with thermistors, and the need for a reference temperature. Thermocouples are characterized by a larger linearity than thermistors, but a smaller linearity than RTDs. Unlike thermocouples, RTDs, ICs, and negative temperature coefficient of resistance (NTCR) thermistors are passive sensors that require current excitation to produce a voltage output, which becomes larger than that given by thermocouples. Modern Si- and Ge-based semiconductors are often integrated into multifunction ICs, which offer reasonable accuracy and high linearity over an operating temperature range of −55° to 150°C, as listed in Table I.

In some industrial applications below 600°C, RTDs are replacing thermocouples. Nevertheless, when compared with NTCR thermistors, platinum RTDs are less sensitive to small temperature changes, and have a much slower response time, as indicated in Table I. In fact, thermistors' high sensitivity (typically between −2%/°C and −6%/°C, at 25°C), Fig. 1, allows the detection of minute variations in temperature, which sometimes could not be observed with an RTD or thermocouple. The lack of interchangeability of thermistors was once one of the major factors against their widespread use, but nowadays thermistors can match manufacturer's calibration curves to ±0.1°C. Thermistors' accuracy can be as good as ±0.001°C,

D. J. Green—contributing editor

Manuscript No. 25362. Received October 15, 2008; approved January 15, 2009.
Antonio Feteira is a Visiting Lecturer in the Department of Engineering Materials at The University of Sheffield.
†Author to whom correspondence should be addressed. e-mail: antonio.feteira @epcos.com; a.feteira@sheffield.ac.uk
‡This term is actually a contraction of the words "thermal resistor", which was proposed by the Bell Telephone Laboratories in the early 1940s.

Review

**Table I. Characteristics of Temperature Sensors**

| Characteristics | Thermocouple | RTD | Thermistor | Integrated circuit |
|---|---|---|---|---|
| Active material | Two dissimilar metals | Platinum | Ceramic | Si or Ge |
| Changing parameter | Voltage | Resistance | Resistance | Voltage or current |
| Temperature range [°C] | −270 to +2300 | −200 to +650 | −50 to +1000 | −55 to +150 |
| Additional circuitry | Reference junction | Lead compensation | Linearization | Linearization |
| Sensitivity | ~1–80 μV/°C | ~0.4%/°C | −2%/° to −6%/°C | −7.3%/°C (Si)<br>−5%/°C (Ge) |
| Accuracy [±°C] | 0.5–5 | 0.001–1 | 0.001–1 | 1 |
| Response time | Fast, 0.1–10 s | Slow, 1–50 s | Fast, 0.1–10 s | Fast, <0.1 s |
| Stability | Moderate | Excellent | Moderate | High |
| Cost | Low | Moderate to high | Low to moderate | Low |
| Advantages | Wide operating temperature range,<br>Low cost,<br>Rugged | Linearity,<br>Wide operating temperature range,<br>Highest stability | Fast response time,<br>Low cost,<br>Small size,<br>Large changes in resistance versus temperature | Highly linear,<br>Low cost |
| Disadvantages | Nonlinear,<br>Low sensitivity,<br>Reference junction compensation required,<br>Subject to electrical noise | Slow response time,<br>Expensive,<br>Current source required,<br>Sensitive to shock | Nonlinear,<br>Current source required,<br>Currently, limited temperature range | Very limited temperature range,<br>Power source required |

but most commercial applications have an accuracy of ±0.1°C. The majority of commercial NTCR thermistors are ceramic semiconductors based on transition-metal oxides such as NiO, CoO, MnO, etc. In order to fulfill the requirements imposed by each specific application, most electroceramic manufacturers offer thermistor components in a wide variety of designs, ranging from surface-mounted to radial or axial leaded packages, as illustrated in Fig. 2. The electrical characteristics of these components can be geometrically and chemically tailored to meet specific requirements.

Hereafter, this review is devoted to NTCR ceramic thermistors. First, a historical perspective of the commercial implementation of NTCR thermistors is given. The most significant and recent patents in the field of NTCR thermistors are reviewed alongside scientific discoveries that lead to a better understanding of NTCR behavior. This is followed by an extensive description of the crystal-chemistry of spinels and perovskites compounds, the current materials of choice for the fabrication of NTCR ceramics. Then, mechanisms of electrical conductivity in solids are briefly revised, with particular emphasis on mechanisms responsible for semiconductivity in NTCR ceramics. Other physical characteristics exhibited by NTCR thermistors are also addressed. Considering that the performance of NTCR ceramic thermistors (in particular, their stability) is strongly dependent on processing conditions, this topic is reviewed here from an industrial viewpoint. Examples of the most common applications of NTCR thermistors in modern electronics are presented. This review concludes with an outlook on the exciting future possibilities and scientific challenges in the field of NTCR thermistors. Hopefully, this will encourage further investigations into NTCR ceramics.

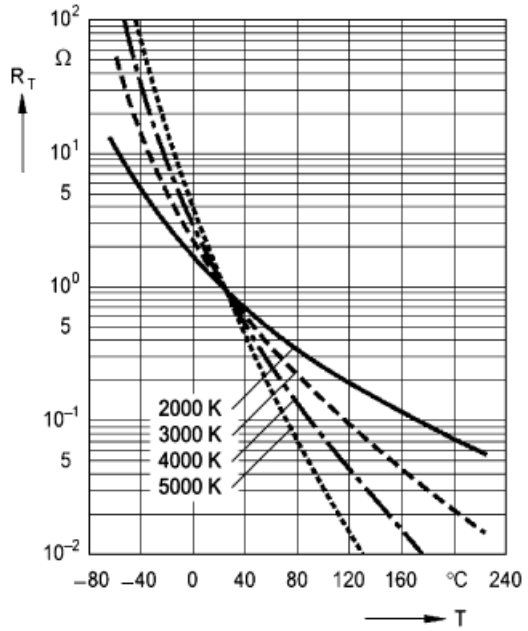


**Fig. 1.** Schematic representation of the temperature dependence of resistance for NTCR thermistors. NTCR, negative temperature coefficient of resistance (Courtesy from EPCOS AG, Germany).

## II. Historical Development of NTCR Thermistors

NTCR ceramic thermistors are ubiquitous in modern electronics, where they are used for temperature monitoring, control, and compensation; therefore, not surprisingly, they constitute an important business segment for most electroceramic manufacturers. Historically, much of the research conducted on NTCR thermistors was led by the industry, a situation that still persists today. A chronological listing of events that lead to the mass production of NTCR ceramics is given below. This is not an exhaustive inventory, however, from the author's viewpoint, it compiles most of the relevant discoveries and advances in the field.

The first evidence for the NTCR behavior was registered on February 21, 1833 by the English natural philosopher Michael Faraday, who observed the resistance of silver sulphide, $Ag_2S$, to decrease with increasing temperature. On his own words, "There is no other body with which I am acquainted, that like sulphuret of silver, can compare with metals in conducting power for electricity at low tension when hot, but which, unlike them, during cooling, loses power, whilst they, on contrary, gain."[2] Nevertheless, this phenomenon remained a mere scientific curiosity for nearly 100 years, until the observation of similar response in transition-metal oxides such as $Fe_3O_4$, CoO, and NiO.[§]

[§]Nominally pure stoichiometric NiO (pale green) is actually an excellent insulator, with a room temperature resistivity in excess of $10^{13}$ Ωcm. Nevertheless, non-stoichiometry induced by oxygen uptake at temperatures as high as 1000°C converts NiO into a black conductive solid, which shows p-type semiconductivity. Similar behavior is observed for CoO. On the other hand, $Fe_3O_4$ is an n-type semiconductor.

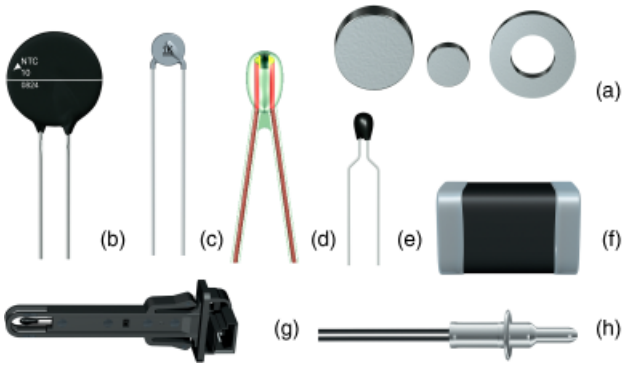


**Fig. 2.** Examples of NTCR components: (a) leadless, (b,c) lead space, (d) glass-encapsulated, (e) resin-encapsulated, (f) SMD, and (g,h) probe sensors. (Courtesy from: EPCOS AG, Germany). NTCR, negative temperature coefficient of resistance; SMD, surface-mounted device.

This discovery prompted the design of novel instruments, whose fundamental operation was based on the NTCR behavior. For example, on March 18, 1930, Samuel Ruben (the cofounder of Duracell) filled the first patent,[3] detailing the fabrication of an electrical pyrometer device based on cuprous oxide ($Cu_2O$), as illustrated in Fig. 3. In the same document, he also suggested the use of fused mixtures of $Cu_2S$ (halbschwefelkupfer) and $Sb_2S$ to fabricate temperature measurement devices. In 1933, Andres[4] proposed the adjustment of the electrical resistance of CuO, MnO, CdO ceramics either through heat treatments, preferably under a hydrogen atmospheres, or by the application of high voltages.

In 1935, the Dutch company Koninklijke Philips Electronics N.V. (vulgarly refered to as Philips) presented a "novel" NTCR product, which would be traded under the name "Starto."[5] This material consisted basically of a mixture of Hattenleidelheimer clay[¶] with semiconductive silicon or other substance having similar characteristics, such as ferrosilicon. The idea behind the combination of these two materials was threefold. First, increase simultaneously the room temperature resistance and the temperature coefficient of electrical resistance of Si-based components. Second, use a ceramic composite approach to tailor these properties, by simply changing the ratio of components and the firing procedure. Third, create a material easily molded to any desired shape, which would offer superior mechanical properties than the resistors available at the epoch. Unfortunately, in practical terms, Starto components turned out to be less satisfactory than expected. Indeed, these ceramic composites suffered from all sorts of drawbacks: (i) the resistance was extremely sensitive to small fluctuations in the mixing ratio and very difficult to reproduce, (ii) a nonhomogeneous distribution of Si would concentrate the current along certain paths, which eventually resulted in short-circuiting as a result of local heating, and (iii) in order to prevent oxidation of silicon during fabrication, sintering had to be carried out in an atmosphere consisting of a mixture of nitrogen and 10%–30% hydrogen at temperatures as high as 1300°C.

Also in 1935, Walter Schottky from Siemens filled a patent pertaining to the fabrication of a thermonegative resistor, but in this case the device was built from a homogeneous ceramic based on either CuO or $UO_2$.[6] In principle, this approach would circumvent most of the already mentioned shortcomings associated with the composite materials. No preferential paths for current flow would exist and the level of conductivity in these single-phase ceramics should be simply determined by their nonstoichiometry. In practice, this approach proved also difficult, because reproducible adjustment to a certain resistivity was faced with insurmountable obstacles. Moreover, the slightest change in the material's stoichiometry during operation resulted in relatively large changes in resistivity.

[¶]Hattenleidelheimer clay is of German origin with the approximate chemical composition as follows: 36.2% $SiO_2$, 38.8% $Al_2O_3$, 2.2% $Fe_2O_3$, 0.8% $TiO_2$, 0.6% CaO, 0.2% $Na_2O$, and 1.5% $K_2O$.

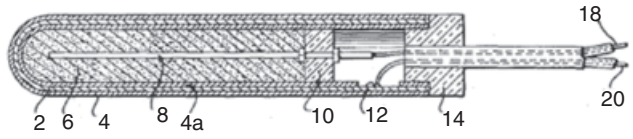


**Fig. 3.** Cross section representation of the pyrometer element patented by Samuel Ruben in 1930. The temperature sensor parts in this device are numbered as (4) and (4a) and consist of oxidized copper, i.e. $Cu_2O$.

In the late 1930s, the Bell Telephone Laboratories also embarked on the commercial exploitation of the NTCR behavior exhibited by spinel-structured ceramics. These relatively inexpensive ceramics were based on mixtures of oxides of manganese and iron or oxides of nickel and manganese. Nevertheless, Becker *et al.*[7] called attention to the discouraging fact that the resistance of some of these ceramics could vary by 3–6 orders of magnitude, depending on the preparative heat treatments. Hence, most of the work carried out at Bell Labs attempted to overcome these shortcomings, by investigating new materials and processing procedures, which would eventually render improved stability and reproducibility. This reproducibility difficulty led a number of European and American manufacturers to adopt the Ni–Mn–Cu oxide system. Ceramics from this system, sintered in open air, exhibited acceptable reproducibility. On the other hand, ceramics based on Co–Fe were not so amenable to air heat treatments and required stabilization by doping or tighter control of the sintering atmosphere.[8]

By the late 1940s, thermistors could be found in important and large scale uses, such as in telephone centrals and military equipment. Some of the functions of NTCR ceramics included time delay and device protection, voltage regulation, speech volume limitation, testing equipment for ultrahigh frequency power, and detection of very small radiant power. In all these applications, thermistors were chosen because they were simple, small, rugged, had a long life, and required little maintenance. In 1939, Bell Labs introduced the so-called "high speed thermistor,"[9] i.e. a thermally sensitive resistor capable of closely following audio or high frequency variations of voltage. This invention was basically a design concept based on the deposition of $UO_2$ dense ceramic films (with a thickness of $\sim$1 mm) onto a platinum foil. This new design exhibited enhanced heat transfer characteristics in comparison with their bulk counterparts, and could be operated at frequencies up to 17 kHz.

Nevertheless, the most influential work in the field of NTCR ceramics thermistors in the late 1940s can probably be credited to Verwey and his colleagues from the Philips Research Laboratories. They carried out extensive investigations on the structure–composition–property relationships in spinel-structure ceramics.[10–19] Their rationalization of the conductivity behavior in $Fe_3O_4$, based on an electron hopping mechanism (see Section IV(*l*)), constituted a turning point in the understanding of NTCR behavior. From this discovery came the need to understand how spinel-structured transition-metal oxides behave when combined with other metal oxides. Although the three aforementioned companies were heavily engaged in developing reproducible and stable NTCR ceramics, they were mostly concerned with materials with operation temperatures limited to 300°C. Hence, in 1948, Torok[20] revealed his efforts towards the discovery of NTCR materials usable up to 1200°C. He argued silicates (ceramics or glasses) and carbides were inappropriate, because the first show time-dependent conductivity whereas the second loose carbon at high temperatures. He also discarded most of the transition-metal oxides, because they are chemically unstable (e.g. $Mn_2O_3$) and fail to return instantaneously to any initial conductivity value after being subjected to a temporary temperature change. Nevertheless, among transition-metal oxides, chromic oxide, $Cr_2O_3$, appeared to exhibit an exceptional stability. As pointed out by Torok, $Cr_2O_3$ stoichiometry remains virtually unchanged up to temperatures as high as 1500°C. Furthermore, the resistivity of $Cr_2O_3$ ceramics could be modified through the addition of other metal oxides such as CoO, BaO,

and $Fe_2O_3$. Nevertheless, full densification of $Cr_2O_3$-based ceramics appeared to be extremely difficult to concretize at temperatures lower than 1500°C. Torok suggested that $Bi_2O_3$ could be strategically added as a sintering aid; however, in order to avoid its complete volatilization prior to completion of the initial stage of sintering, it was advisory to increase the temperature rapidly, after debiding.

In the post war era (1950/60), more sophisticated applications were introduced and manufacturing expansion occurred when aerospace and cryogenic devices were introduced. In terms of fundamental research, most work was devoted to the basic structural, electrical, and magnetic characterization of NTCR thermistors based on doped $NiMn_2O_4$ ceramics. These studies aimed to better understand the interplay between cation arrangement and physical properties. For example, Romeijn[21] from Philips Laboratories complemented Verwey's work through an exhaustive characterization of the physical and crystallographic properties of several spinels.

From the above, it becomes evident that most of the research into NTCR ceramics was conducted almost exclusively by the industry; however, this situation changed gradually from the 1950s onwards. For example, John Goodenough's research has contributed substantially to the understanding of the electronic properties of transition-metal spinels and perovskites.[22–29] Crystallographic and magnetic studies of the system $(1-x)NiFe_2O_4$–$(x)NiMn_2O_4$ were also carried out by Baltzer and White[30] in 1957. In the same year, Dunitz and Orgel[31,32] investigated the electronic properties of transition-metal oxides, with special emphasis on spinels (e.g., $CuFe_2O_4$, $CuCr_2O_4$, $ZnMn_2O_4$, and $NiCr_2O_4$) and perovskites (e.g., $BaTiO_3$, $KNbO_3$, and $LaMnO_3$). They stressed that most of the physical and crystal chemistry of these oxides could, in fact, be rationalized by the application of the crystal field theory, as previously proposed by other researchers such as Romeijn.[21] The oxidation behavior of $MnFe_2O_4$ in air between 750° and 1150°C was studied by Weitz, who observed the decomposition of this material at 1050°C according to the reaction $4\ MnFe_2O_4 + O_2 \leftrightarrow 2\ Mn_2O_3 + 4\ Fe_2O_3$.

In 1964, Wickham[33] from the Ampex Computer Products Company published a complete study on phase equilibria in the $NiO–Mn_2O_3–O_2$ system. In this work, the phase relationships in air and pure oxygen were presented. In 1969, the same author published a similar study devoted to the $Fe_2O_3–Mn_2O_3$ system.[34] In the 1970s, the interest in high-temperature NTCR ceramics was revived by companies such as Ford Motor Corporation,[35] Matsushita Electric Industrial Co., Ltd,[36,37] and Siemens.[38] Nevertheless, these companies added another level of sophistication to the previous requirements imposed onto NTCR ceramics. Ford was particularly interested in NTCR ceramics in which resistivity was virtually independent of oxygen partial pressure, so that they could be used in the exhaust gas of internal combustion engines. $PrFeO_3$ and other $RFeO_3$ (where R is a rare-earth) perovskites exhibited the appropriate characteristics for the fabrication of temperature sensors that could be operated in a variable oxygen atmosphere.[35] E. I. Du Pont de Nemours and Company filled several patents,[39] which for the first time suggested the use of semiconductive pyrochlores to fabricate NTCR thermistors. Also in the 1970s, greater emphasis on sensor stability and performance resulted in better sensor housing designs. For example, in 1973, Shibaura Electronics Co. Ltd. initiated the commercialization of glass-encapsulated thermistors. Thermistor manufacturers began to focus on volume production and high accuracy, reaching an annual production of 50 million units. During this decade, Brabers from the Eindhoven Institute of Technology investigated in detail the ionic configuration and the electrical properties of $Ni_xMn_{3-x}O_4$, $Mn_xFe_{3-x}O_4$, and $Cu_xMn_{3-x}O_4$ ceramics.[40–45] The growing practical and commercial importance of NTCR ceramics was accompanied by the publication of a book entitled "Thermistors" by E. D. Macklen.[8]

In the 1980s, TDK Corporation revisited the "Starto concept" to create high-temperature (400°–800°C) thermistors. Nevertheless, in this approach, instead of Hattenleidelheimer clay, the insulator matrix was a pure insulator oxide such as $Al_2O_3$, $SiO_2$, or MgO, whereas the conductive phase was a carbide compound such as SiC or BC.[46] Also in the 1980s, Dorris and Mason[47] carried out a comprehensive study devoted to the high-temperature cation distribution and electrical properties of $Mn_3O_4$. Their electrical and thermopower measurements confirmed a small-polaron model of electronic conductivity. They also explained the electrical behavior of $NiMn_2O_4$ and $CuMn_2O_4$ based on the disproportion equilibrium $2Mn^{3+}_{oct} \Leftrightarrow Mn^{4+}_{oct} + Mn^{2+}_{oct}$, which governs the $Mn^{4+}$ and $Mn^{3+}$ concentrations in $Mn_3O_4$. In 1985, Macklen[48] from STC components revisited the electrical properties and cation distribution in $NiMn_2O_4$ ceramics. He presented a critical review of the cation configuration models proposed by previous investigators.

In the beginning of the 1990s, several University-based research groups became extraordinary active in the field of NTCR ceramics.[49–59] A special reference should be made to the French research group based at the Université Paul Sabatier. This group not only used several distinct research techniques to provide a better understanding of the aging of electrical properties, as described in Section IV(*3*), but also investigated new processing routes for NTCR ceramics, as described in Section V.

In 1997, Groen from Philips Corporation filled a patent pertaining to the fabrication of a high-temperature thermistor ceramic entirely based on rare-earth oxides, which could be used from room temperature up to 1000°C. This novel ceramic system was prepared according to the formula:[60] $Y_aGd_bSm_cTb_dO_3$, wherein $0 \le a, b, c \le 0.995$, $0.01 \le c \le 0.995$, and $a > 0$ if $b = 0$, or $b > 0$ if $a = 0$. In 1999, Feltz *et al.*[61] characterized the structure and electrical properties of several strontium manganate ceramics and proposed $Sr_7Mn_4O_{15}$ to be suitable for high-temperature applications. From 2000 onwards, most research has been devoted to the understanding of the factors that control the stability of NTCR ceramics (see Section IV) and to the development of materials that can withstand higher temperatures and harsher environments. For example, Feltz *et al.*[62] explored the potential of $Sr_xLa_{1-x}Ti_{x+y}Co^{III}_yCo^{II}_{1-x-2y}O_3$ perovskite-structured ceramics for high-temperature applications. Novel powder processing routes for NTCR ceramics were also experimented and reported, as discussed later in Section V. During the last decade, the production of NTCR thermistor films has attracted considerable attention, as reflected by the increasing number of publications on doped $NiMn_2O_4$ films.

## III. Crystal-Chemistry of NTCR Ceramics

Despite the large number NTCR components offered by electroceramic manufacturers, these components revolve around a surprisingly small number of crystal structure-types. Nevertheless, their resistance–temperature characteristics can vary significantly with the composition and processing conditions. Hereafter, we present the most relevant structural families used in the manufacture of NTCR components.

### *(1) Spinels*

The term spinel refers to the mineral $MgAl_2O_4$ and it is used in mineralogy to refer to the entire group of very similar minerals with the general formula $AB_2O_4$. The crystal structure of spinel has long been determined independently by Bragg[63,64] and Nishikawa[65] to be described by the cubic space group *Fd3m* (number 228 in the International Table of X-ray crystallography). This structure can be approximately described by a cubic close packing of large $O^{2-}$, with $Mg^{2+}$ and $Al^{3+}$ occupying interstices. In this closed-packed structure there are 64 tetrahedral (A-sites) and 32 octahedral (B-sites) interstices. Each unit cell contains eight $[MgAl_2O_4]$ formula units and therefore 32 $O^{2-}$, 8 $Mg^{2+}$, and 16 $Al^{3+}$ ions. Hence, half of the octahedral interstices are filled with $Al^{3+}$ ions, whereas only a quarter of the tetrahedral interstices are filled with $Mg^{2+}$ ions. The occupied sites are arranged in such a way that tetrahedral sites share corners with octahedral sites, and the octahedral sites share edges

with each other. The B–B, A–A, and A–B bond lengths in spinels are given by $\frac{\sqrt{2}a_0}{4}$, $\frac{\sqrt{3}a_0}{4}$, and $\frac{\sqrt{11}a_0}{8}$ where $a_0$ is the lattice constant. The shorter B–B bond lengths play a fundamental role in the electrical conductivity mechanism operating in these materials, as discussed in Section IV(*1*).

In 1932, Barth and Posnjak[66] point out that many spinels could accommodate significant amounts of cation disorder, i.e. they proposed an alternative cation distribution, in which the cubic symmetry was still preserved. Later, Verwey and Heilmann[15] introduced the terms "normal spinel" and "inverse spinel" to designate the limiting configurations of cations in spinel-structured compounds. In normal spinels, the cation distribution is given by the formula $[A]^{tet}[B_2]^{oct}O_4$, i.e. A and B cations occupy tetrahedral and octahedral sites, respectively. In inverse spinels, the cation distribution is given by the formula $[B]^{tet}[A,B]^{oct}O_4$, i.e. half of the B cations occupy tetrahedral sites, whereas the other half of the B cations and all of the A cations occupy the octahedral sites.

Often, A and B cations are disordered over the octahedral sites, and a complete range of intermediate cation distributions is possible, which can also be temperature dependent. The cation distribution is normally quantified by a parameter, $\gamma$, which basically is the fraction of A ions on the octahedral sites. Obviously, this parameter has the values 0 and 1 for normal and inverse spinels, respectively, whereas for a random spinel, $[B_{0.67}A_{0.33}]^{tet}[A_{0.67}B_{1.33}]^{oct}O_4$, $\gamma$ is equal to 0.67. Several factors influence $\gamma$, including the site preferences of ions in terms of size, covalent bonding effects, and, especially, the crystal field stabilization energies (CFSE).

The crystal field theory has proved to be a particularly useful tool for establishing the relationships between chemical composition, crystal structure, and properties of transition-metal oxides, in particular of spinels and perovskites. This theory starts from the electronic state of free ions (*in vacuo*) and deals with the effects of the surrounding ions (ligand) on the coordination environment of the central ion. When a transition-metal ion is surrounded by six negative ions (e.g. oxygen), the five *d* orbitals are no longer degenerate (same energy), but split into two groups, a lower energy triplet, $t_{2g}$, and an upper energy doublet, $e_g$. The physical basis for this splitting is simply the electrostatic repulsion between the *d* electrons and the surrounding negative ions. The $e_g$ ($d_{z^2}, d_{x^2-y^2}$) orbitals point directly at the oxygen ions and are destabilized. On the other hand, the $t_{2g}$ ($d_{xy}$, $d_{xz}$, $d_{yz}$) orbitals point between the oxygen ions and are therefore stabilized. The crystal field splitting of energy in transition-metal oxides may result in CFSE, which depend upon the number of *d* electrons and the symmetry of the crystal field. The energy difference, $\Delta$, between $t_{2g}$ and $e_g$ is set to be 10 Dq. The $t_{2g}$ orbitals are stabilized by 4 Dq, whereas the $e_g$ orbitals are destabilized 6 Dq. The CFSE can be simply calculated in relation to five degenerate *d* orbitals without crystal field splitting. This can be made clear by considering a few examples. The electron distribution of $Cr^{3+}$ in an octahedron is $t_{2g}^3e_g^0$. The energy gain resulting from three electrons in the low energy $t_{2g}$ orbitals is $3 \times 4$ $Dq_{oct} = 12$ $Dq_{oct}$. For $Mn^{3+}$ in an octahedron ($t_{2g}^3e_g^1$) the stabilization is given by $3 \times 4$ $Dq_{oct} - 1 \times 6$ $Dq_{oct} = 6$ $Dq_{oct}$.

For certain electron configurations, additional crystal field stabilization can be obtained by deforming the environment of the metal ion. The Jahn-Teller effect is responsible for these distortions in $d^9$, $d^7$ (LS), and $d^4$ (HS) ions. For example, for $d^9$ ion $Cu^{2+}$ with the $t_{2g}^6e_g^3$ configuration, one of the $e_g$ orbitals contains two electrons and the other contains one electron. Because the $e_g$ orbitals point directly to the oxygen ions, the double occupied orbital experiences stronger repulsions, which results in the lengthening of the metal–oxygen bonds in the direction of this orbital. For example, if the $d_z^2$ orbital is doubly occupied, the two metal–oxygen bonds along the *z* axis are longer than the other four bonds. The structure of many spinels of $Cr^{2+}$ ($d^4$), $Mn^{3+}$ ($d^4$), and $Cu^{2+}$ ($d^9$) is deformed by the Jahn-Teller effect.[67]

The cation distribution in spinels and the degree of inversion, $\gamma$, have been studied in considerable detail, as presented below for three selected compounds: $Fe_3O_4$ (Magnetite), $Mn_3O_4$ (Hausmannite), and $NiMn_2O_4$. Variations on the distribution of cations in the A and B positions cause some remarkable changes in some of the physical properties, such as electrical conductivity and thermopower.

At room temperature, $Fe_3O_4$ was described by Verwey and Haayman[14] as possessing an inverse spinel structure, given by the formula $Fe^{3+}[Fe^{2+}Fe^{3+}]O_4$, where the square brackets represent the octahedra site. This cation distribution has been proposed to explain the high electrical conductivity exhibited by $Fe_3O_4$. Nevertheless, at high temperatures ($\sim$1500°C), a random cation distribution $Fe_{0.33}^{2+}Fe_{0.67}^{3+}[Fe_{0.67}^{2+}Fe_{1.33}^{3+}]O_4$ was suggested by several investigators. In 1981, Wu and Mason[68] used thermopower measurements in the temperature range 600° to 1500°C to determine the exact cation distribution in stoichiometric $Fe_3O_4$ as a function of temperature. They observed the cation distribution to vary from inverse at low temperatures to random at $\sim$1450°C, as illustrated in Fig. 4.

Moreover, Wu and Mason[68] proposed an "equilibrium" room-temperature cation distribution given as $Fe_{0.0004}^{2+}Fe_{0.9996}^{3+}$-$Fe_{0.9996}^{2+}Fe_{1.0004}^{3+}]O_4$, which appears to be in agreement with the $Fe_{0.025}^{2+}Fe_{0.975}^{3+}[Fe_{0.975}^{2+}Fe_{1.025}^{3+}]O_4$ distribution determined from magnetic measurements.

At high temperatures (>1170°C), $Mn_3O_4$ has a cubic spinel structure, but at low temperatures it is stable as a tetragonally distorted spinel. Distinct differences exist between the electrical properties of these two forms of $Mn_3O_4$. Upon the transformation from tetragonal to cubic, the resistivity decreases by 1–2 orders of magnitude, with a concurrent decrease in the activation energy from 1.3 eV in the tetragonal phase to 0.65–0.75 in the cubic phase.[69] The exact cation valence distribution in $Mn_3O_4$ was a matter of controversy for many years. Early researchers proposed a $Mn^{2+}[Mn^{4+}Mn^{2+}]O_4$ configuration,[21] whereas later studies favored a $Mn^{2+}[Mn^{3+}Mn^{3+}]O_4$ structure.[69] In these two models, both $Mn^{3+}$ and $Mn^{4+}$ show preferential occupation of the octahedral site; therefore, their tetrahedral concentration is expected to be very small. Additionally, the tetragonal distortion can be attributed to the presence of $Mn^{3+}$ in the octahedra, because of its $3d^4$ electronic configuration. On the basis of the aforementioned, it is reasonable to expect a $Mn^{2+}[Mn^{3+}Mn^{3+}]O_4$ cation valence distribution to $Mn_3O_4$. Nevertheless, this model is inconsistent with the high conductivity exhibited by cubic $Mn_3O_4$. Alternatively, Dorris and Mason[47] proposed that the cubic structure is described by a $Mn_1^{2+}[Mn_z^{2+}Mn_{2-2z}^{3+}Mn_z^{4+}]O_4$ cation valence configuration, where z is the so-called "degree of disproportionation." Basically, the concentrations of $Mn^{4+}$ and $Mn^{3+}$ are

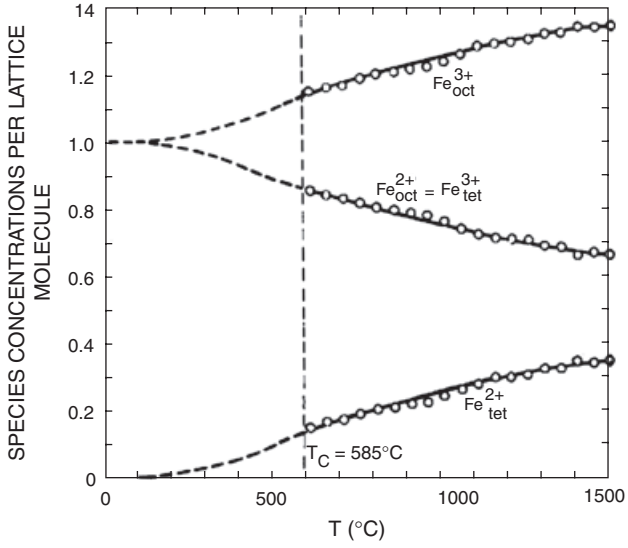


**Fig. 4.** Temperature dependence of the cation distribution in magnetite, calculated from Seebeck coefficient analysis. The theoretical behavior has been extrapolated to temperatures below $T_c$. (After Wu and Mason[68]).

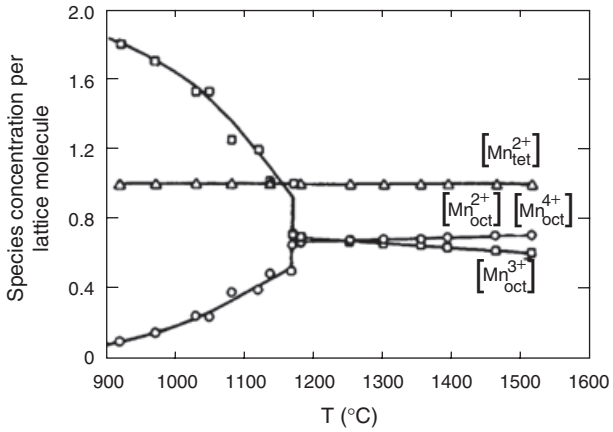


**Fig. 5.** Cation distribution in $Mn_3O_4$ as a function of temperature. (After Dorris and Mason[47]).

related through a disproportionation equilibrium, given as $2Mn^{3+}_{oct} \Leftrightarrow Mn^{2+}_{oct} + Mn^{4+}_{oct}$. This is a known reaction in aqueous solutions. Based on thermopower analysis, which assumed an electron hole $Mn^{4+}/Mn^{3+}$ conduction mechanism, Dorris and Mason[47] proposed a cation distribution for $Mn_3O_4$, as represented in Fig. 5. The disproportionation reaction also affords an appropriate description of the cubic-to-tetragonal transformation as the temperature decreases. The octahedral $Mn^{3+}$ responsible for the tetragonal distortion increases in concentration with decreasing temperature. Hence, at a critical concentration, $Mn_3O_4$ will adopt the tetragonal structure. At low temperatures, $Mn_3O_4$ will be eventually described by a $Mn^{2+}[Mn^{3+}Mn^{3+}]O_4$ configuration, as suggested by the temperature dependence of $[Mn^{3+}_{oct}]$ in Fig. 5.

Nowadays, most NTCR ceramics are based on $Mn_3O_4$ ceramics, where $Mn^{3+}$ is partially replaced by other transition-metals such as Ni, Co, Fe, and Cu in order to induce semiconductivity in this rather resistive material. These substitutions lead to the formation of $Mn^{3+}/Mn^{4+}$ pairs on the octahedral sites, which are essential for electrical conductivity, as discussed in Section IV(*1*).

$NiMn_2O_4$ is definitely the most studied spinel for NTCR applications. This compound is unanimously recognized as an inverse spinel; however, the exact nature of the valences and distribution of the cations have proved to be controversial. Different configurations have been suggested by several investigators, depending on their choice of characterization techniques or even methods of preparation and calcination temperatures. Most of these configurational models suggested to date are listed in Table II. Although certain configurations could account for the magnetic behavior, they failed to explain the experimental electrical data, which require the coexistence of $Mn^{3+}$ and $Mn^{4+}$ on the B-sites. Nevertheless, it is also unanimously accepted that the degree of inversion in $NiMn_2O_4$ decreases with increasing temperature.

Although there is no clear agreement on the exact valence distributions of other spinels such as $NiCo_2O_4$ or $NiFe_2O_4$, in most cases authors agree on some basic facts: $Co^{3+}$ prefers octahedral coordination, whereas $Co^{2+}$ occupies mainly, but not exclusively, tetrahedral sites.[56] On the other hand, iron, found predominantly as $Fe^{3+}$, when in low concentrations shows no strong site preference, but in high concentrations ($x > 0.4$) preferentially occupies octahedra. A comprehensive review on the configurational models of spinels will be presented elsewhere. In summary, the inverse spinel structure of $Fe_3O_4$ it is a manifestation of the intersite exchange reaction, $Fe^{2+}_{tet} + Fe^{3+}_{oct} \Leftrightarrow Fe^{2+}_{oct} + Fe^{3+}_{tet}$. According to O'Neill and Navrotsky, the $Fe^{2+}/Fe^{3+}$ exchange is energetically favorable, whereas the $Co^{2+}/Co^{3+}$ and $Mn^{2+}/Mn^{3+}$ are energetically unfavorable. Hence, an octahedral disproportionation reaction, $2Mn^{3+}_{oct} \Leftrightarrow Mn^{2+}_{oct} + Mn^{4+}_{oct}$, was proposed to occur in $Mn_3O_4$. The fact that these oxides obey different defect reactions affects decisively their electrical behavior. The exact defect reaction occurring in $NiMn_2O_4$ has been a matter of debate. In fact, both reactions are referred in the literature.

Finally, in $Ni_{1-x}Mn_{2+x}O_4$, the transition from cubic to tetragonal occurs at $x = 0.43$. This transition is driven by the increase of $Mn^{3+}$ ions on the B-site. At a large enough $Mn^{3+}$ concentration, the cooperative long range interaction of distorted octahedra results in a macroscopic tetragonal symmetry, as a result of the aforementioned Jahn-Teller effect. This transformation induces stress in the grains of the ceramic, which is relieved by the appearance of ferroelastic domains.

### *(2) Perovskites*

In general, the term perovskite refers to compounds represented by the formula $ABO_3$, which are isostructural with $CaTiO_3$.

**Table II. Valence Configuration Models Proposed for $NiMn_2O_4$**

| Year | Investigators | Techniques | Cation distribution |
|---|---|---|---|
| 1957 | Bongers[128] | Magnetic measurements | $Mn^{2+}[Ni^{2+}Mn^{4+}]O_4^{2-}$ |
| 1957 | Sinha *et al.*[129,130] | XRD | $Mn^{2+}[Ni^{2+}Mn^{4+}]O_4^{2-}$ |
| 1958 | Baltzer and White[30] | XRD and Magnetic measurements | $Mn^{2+}[Ni^{2+}Mn^{4+}]O_4^{2-}$ |
| 1959 | Azároff | Neutron diffraction | $Mn^{3+}[Ni^{2+}Mn^{3+}]O_4^{2-}$ |
| 1961 | O'Keefe[131] | Crystal field theory | $Mn^{2+}_x Mn^{3+}_{1-x}[Ni^{2+}_{1-x}Mn^{3+}_{1-x}]O_4^{2-}$ |
| 1962 | Larson *et al.*[82] | XRD, electrical conductivity, Seebeck, and magnetic measurements | $Mn^{2+}_{0.65}Mn^{3+}_{0.35}[Ni^{2+}Mn^{3+}_{0.35}Mn^{4+}_{0.65}]O_4^{2-}$ |
| 1969 | Boucher *et al.*[132] | Magnetic and neutron measurements | $Ni^{2+}_{1-y}Mn^{3+}_y[Ni^{2+}_v Mn^{3+}_{2-v}]O_4^{2-}$ |
| 1972 | Brabers[133] | Infrared | $Mn^{2+}_y Ni^{2+}_{1-y}[Ni^{2+}_y Mn^{3+}_{2-2y}Mn^{4+}_y]O_4^{2-}$ |
| 1976 | Bhandage and Keer[134] | XRD, ESR, electrical conductivity, and Seebeck measurements | $Mn^{3+}[Ni^{2+}Mn^{2+}_{0.1}Mn^{3+}_{0.9}]O^{2-}_{3.95}$ |
| 1982 | Brabers and Terhell[135] | Electrical conductivity, thermopower, and thermal expansion measurements | $Ni^{2+}_{1-v}Mn^{2+}_v[Ni^{2+}_v Mn^{3+}_{2-2v}Mn^{4+}_v]O_4^{2-}$ |
| 1983 | Brabers *et al.*[136] | X-ray photoelectron spectroscopy | $Ni^{2+}_{1-v}Mn^{2+}_v[Ni^{2+}_v Mn^{3+}_{2-2v}Mn^{4+}_v]O_4^{2-}$ |
| 1986 | Macklen[48] | Electrical measurements and thermobalance | $Ni^{2+}_{0.35}Mn^{2+}_{0.65}[Ni^{2+}_{0.65}Mn^{3+}_{0.70}Mn^{4+}_{0.65}]O_4^{-2}$ |
| 1987 | Golestani *et al.*[137] | X-ray diffraction | $Ni^{2+}_{0.17}Mn^{2+}_{0.83}[Ni^{2+}_{0.49}Mn^{3+}_{1.66}]O_4^{-2}$ |
| 1988 | Islam and Catlow[138] | Computational methods | $Ni^{2+}_{1-v}Mn^{3+}_v[Ni^{2+}_v Mn^{3+}_{2-2v}]O_4^{2-}$ |
| 1997 | Laberty *et al.*[139] | Wide angle X-ray scattering | $Ni^{2+}_{0.21}Mn^{2+}_{0.29}\nabla_{0.5}[Ni^{2+}_{0.37}Ni^{3+}_{0.25}Mn^{4+}_{1.37}]O_4^{2-}$ |

XRD, X-ray diffraction.

Nevertheless, the ideal cubic perovskite structure is better typified by $SrTiO_3$, which possesses a primitive cubic unit cell with a lattice constant $a = 3.905$ Å and space group $Pm\bar{3}m$ (space group No. 221). This structure consists of closed-packed $AO_3$ layers, with 1/4 of the octahedral interstices occupied by the B cations. The tetrahedra in this structure are empty, decreasing its degree of complexity in relation to spinels. In principle, this feature is the main advantage offered by the perovskite structure over the spinel structure. This allows a more straightforward control of cation disorder and, consequently, of the electrical characteristics. Basically, site occupancy can be predicted to a certain extent from the ionic radii. Hence, large ions such as Ba, Sr, Ca, and Y are almost exclusively present on the A-site, and smaller ions on the B-site. There are few ions of intermediate ionic radii, which shows a so-called amphoteric behavior in large unit cells. There are also situations where nanometric phase separation is observed.[70] Similarly to spinels, distortions from cubic symmetry in transition-metal perovskites can be related to the electronic configuration of the metal ion. Hence, the principles of crystal field theory are fully applicable to perovskites. The *d* electrons of transition-metal cations M in the octahedral sites may exhibit localized or itinerant behavior, cooperative Jahn-Teller ordering of either localized-electron orbitals or narrow-band itinerant-electron ordering, and metallic or polaronic conduction.

Although, transition-metal perovskites have been studied for more than half a century, owing to their fascinating electronic and magnetic properties, their potential as NTCRs has been seriously considered only recently. This investigation was prompted by the fact that commercial NTCRs based on spinels are not suitable for high-temperature applications for a number of different reasons such as too low resistivity and activation energy, poor thermal stability (aging, see Section IV(*3*)), etc.

In 1996, Macher *et al.*[71] carried out a critical comparison of perovskite versus spinel for high-temperature applications as NTCRs. They concluded that both materials conduct via the same mechanism. Moreover, they showed that the conductivity of $LaCo_{1-x}M_xO_3$, where M = Al, Ti, can be systematically controlled, enabling a wide application range. Later, in 2000, Feltz[62] reported on the preparation, structure, and electrical properties of $Sr_xLa_{1-x}Ti_{x+y}Co^{III}_yCo^{II}_{1-x-2y}O_3$ $(0<x<1,\ 0<y<(1-x)/2)$ ceramics. These apparently aging-free materials showed useful properties for NTCR applications to temperatures as high as 500°C. In 2002, Gutierrez *et al.*[72] characterized the structure and the electrical behavior of $Y(Mn_{1-x}Ni_x)O_3$ ceramics. They observed a structural phase transition from hexagonal to orthorhombic at $x = 0.2$. Probably, this transition is driven by a progressive reduction in the concentration of $Mn^{3+}$ Jahn-Teller ions, with increasing *x*. A similar observation was made by Veres *et al.*,[73] when investigating the potential of $Y(Mn_{1-x}Fe_x)O_3$ ceramics as NTCR thermistors. Ceramic thick films based on $La_{0.7}Sr_{0.3}Zr_{0.5}Co^{2+}_{0.2}Co^{3+}_{0.3}O_3$, $La_{0.8}Sr_{0.2}Zr_{0.5}Co^{2+}_{0.2}Co^{3+}_{0.3}O_3$, and $CaTi_{0.8}Co_{0.2}O_3$ were investigated by Kulawik *et al.*[74] Based on their data, it appears that the two first materials show NTCR characteristics that are useful for applications only from room temperature to 300°C, whereas the third are useful from 300° to 800°C. In addition, these ceramics showed great stability in terms of electrical properties. Recently, Liu *et al.*[75] investigated the NTCR behavior exhibited by $SrTiO_3$ and $BaBiO_3$ composites. At room temperature, $SrTiO_3$ is an good insulator, whereas $BaBiO_3$, with a monoclinic ($P2_1/n$) structure, is a semiconductor because the half-filled 6*s* band is unstable relative to a disproportionation reaction $2Bi^{4+} \rightarrow Bi^{(4-\delta)+} + Bi^{(4+\delta)+}$. Interestingly, the $Ba_{1-x}K_xBiO_3$ and $BaPb_{1-y}Bi_yO_3$ were reported to show superconductivity at 30 K ($x = 0.4$) and 12 K ($y = 0.3$), respectively. Zhao *et al.*[76] also investigated the NTCR behavior of ceramic composites, but based on a mixture between the $Ni_{0.75}Mn_{2.25}O_4$ spinel phase and the $LaMnO_3$ perovskite phase. Although they have elegantly fitted experimental resistivity values with an effective media model, transfer of this approach to the industry might not be so straightforward, because of reproducibility difficulties. This remark also applies to composites based on $Y_2O_3$ and $YCr_{0.5}Mn_{0.5}O_3$.[77]

### *(3) Pyrochlores*

Oxide pyrochlore compounds have the general formula $A^{III}_2B^{IV}_2O_7$. The space group of the ideal pyrochlore structure is $Fd\bar{3}m$ with eight molecules per unit cell. The structure is composed of a two-cation coordination polyhedron. The A cation (typically ~1 Å in ionic radii) establishes an eightfold coordination with $O^{2-}$ to form scalenohedra (distorted cubes) that contain six equally spaced $O^{2-}$ and 2 other $O^{2-}$ at a shorter. The B cations are smaller (~0.6 Å in ionic radii) and sixfold coordinated with $O^{2-}$. Despite the great chemical versatility exhibited by this structure, only recently have Nobre and Lanfredi[78] reported measurable NTCR behavior in $Bi_3Zn_2Sb_3O_{14}$ at temperatures >400°C.

## IV. Fundamental Characteristics of NTCR Thermistors

### *(1) Electrical Properties of NTCR Thermistors*

*(A) Electrical Conductivity/Temperature Characteristics:* Electrical conductivity in metals is brought by the movement of free electrons, which are always present. In nonmetallic solids, on the other hand, conductivity may be due to either movement of electrons (electronic conductivity) or movement of ions (ionic conductivity). Often both movements take place simultaneously.

In practice, only electronic semiconductors are used as materials for NTCR sensors, because ionic conduction is accompanied by chemical changes and polarization phenomena, which are found to be troublesome. Although the conduction in semiconductors is due to the movements of electrons as it occurs in metals, the mechanism of this phenomenon is essentially different from that in metals.

In general, conductivity is given by $\sigma = ne\mu$, where *n* is the number of current carriers, *e* their charge, and μ their mobility. In metals, the number of charge carriers is large and essentially constant; however, their mobility gradually decreases with temperature as a result of electron–phonon collisions. Consequently, their conductivity decreases with increasing temperature.

The electrical characteristics of Si-based temperature sensors can be explained by the band theory for covalent semiconductors; however, a chemical picture of localized valencies is more appropriate than a band model to explain the conductivity observed in oxide semiconductors. In fact, in oxide semiconductors, the concentration of charge carriers is determined solely by the doping level (i.e. it is temperature independent); however, their mobility is temperature activated. Nonetheless, in both materials the resistivity, ρ, depends on temperature according to

$$\rho(T) = \rho_\infty \exp\left(\frac{E_a}{kT}\right) \tag{1}$$

where $\rho_\infty$ it is the resistivity at infinite temperature (approximately independent of the temperature), *k* is the Boltzmann's constant, and $E_a$ is the activation energy for electrical conductivity. Alternatively, for a thermistor device of fixed dimensions and resistivity, Eq. (1) often appears rewritten as

$$R(T) = A \exp\left(\frac{B}{T}\right) \tag{2}$$

where $A = R_\infty$ is the resistance of the device at infinite temperature (i.e. $1/T = 0$) and *B* is the so-called material constant of a thermistor. Hence, differentiation of Eq. (2) gives the sensitivity coefficient, $\alpha = \frac{1}{R} \cdot \frac{dR}{dT}$, which is equal to $-\frac{B}{T^2}$. This indicates that the temperature sensitivity decreases with increasing temperatures. In most commercial spinel-based NTCR ceramics, the *B*-values vary between 2000 and 5000 K, which imparts room-temperature α values ranging from −2.2 and −5.5%/K, respectively.

NTCR ceramics showing low *B*-values find applications in circuit temperature compensation and cryogenic measurements. For high-temperature applications, large *B*-values and resistivi-

ties are required; otherwise, the sensor shows little sensitivity to changes in temperature. For example, $CaZrO_3$-based thermistors exhibit *B*-values as high as 24 000 K.[79]

The B-value for a given device can be calculated from resistance measurements as follows:

$$B = \frac{\ln\left(\frac{R_1}{R_2}\right)}{\left(\frac{1}{T_1} - \frac{1}{T_2}\right)} \quad (3)$$

where $R_1$ and $R_2$ are the resistances at the temperatures $T_1$ and $T_2$, respectively. Most NTCR manufacturers specify *B*-values between two standard temperatures, usually 25° and 100°C. Other specifications exist, depending on the temperature operational range of the device.

In practice, useful materials for NTCR applications should exhibit activation energies for conduction, i.e. $E_a$, between 0.15 and 0.5 eV. Requirements on resistivity values are not so stringent, because the total resistance of the device can be tailored geometrically. Nevertheless, in order to fabricate small commercial NTCR thermistors with total resistances ranging from a few Ω to kΩ at room temperature, materials with specific resistivities from 1 to 100 MΩcm are required. Interestingly, Petric and Ling[80] suggested that spinels with lower theoretical density show higher resistivity. Nevertheless, this is not a universal rule, as clearly demonstrated by $Co_2O_3$ (6.05 g/cm$^3$), which shows higher resistivity than $CuMn_2O_4$ (5.45 g/cm$^3$). Feltz[81] also commented on a larger molar volume to higher resistivity trend, giving $NiMn_2O_4$ and $CuMn_2O_4$ as examples.

Verwey *et al.*[16] were the first to show that both *B*-values and resistivity of NTCR ceramics could be successfully tailored by chemical doping, as shown in Fig. 6 for the $Fe_3O_4$–$MgCr_2O_4$ system. At room temperature, $Fe_3O_4$ shows a specific resistivity of a few mΩ.cm and a too small α for practical applications. Nevertheless, useful resistances can be obtained by forming a solid solution with the nonconducting $MgCr_2O_4$, $MgAl_2O_4$, and $Zn_2TiO_4$. In contrast, $Mn_3O_4$ is a rather resistive spinel that shows useful electrical properties upon substitution of Mn by Ni according to the formula $Ni_{1-x}Mn_{2+x}O_4$. The conductivity mechanism in $Ni_{1-x}Mn_{2+x}O_4$ switches from *n*-type to *p*-type at $x \sim 0.46$.[82] A compositional conductivity transition from *n*- to *p*-type was also determined by Mason and Bowen[83,84] in the $(1-x)Fe_3O_4$–$xFeAl_2O_4$ system at $x \sim 0.5$.

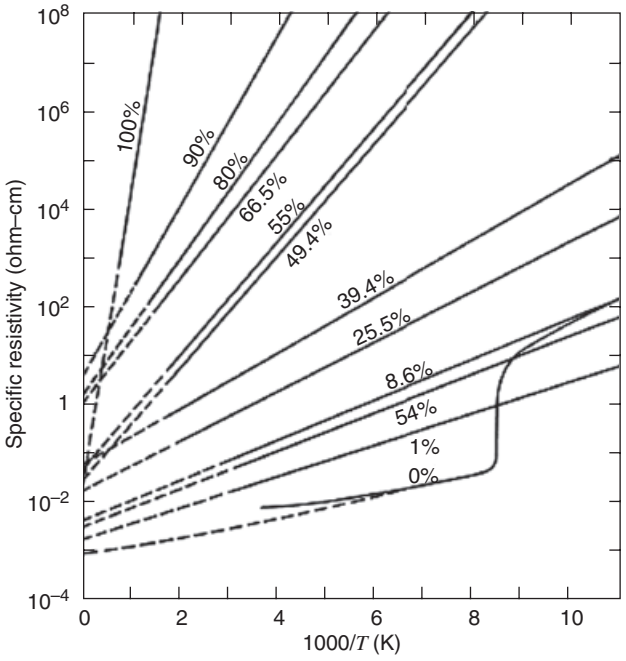


**Fig. 6.** Arrhenius representation of the conductivity versus temperature of $Fe_3O_4$–$MgCr_2O_4$ ceramics. (Adapted from Verwey *et al.*[16])

Although ceramic devices based on $Ni_{1-x}Mn_{2+x}O_4$ ceramics exhibit both stable resistances and *B*-values, they afford limited ranges of both *B*-values and room temperature resistances, $R_{25}$. Hence, in order to achieve higher *B*-values, Fe (or Al) are, for example, added to this system, whereas Co is a possible addition for reducing *B*-values.

Currently, industrially manufactured NTCR ceramics are based on the following oxide systems: Ni–Mn–Cu, Ni–Mn–Cu–Co, Co–Mn–Cu, Fe–Ti, Ni–Li, Co–Li, and Cu–Mn. The addition of other elements such as Fe, Al, Zn, and Mg to modify the electrical characteristics of one of these basic systems is also a common practice.

*(B) Physics of Conductivity:* Microscopically, the electrical conductivity in NTCR ceramics has been interpreted by a small polaron model. Verwey et Haymann[14] interpreted the conductivity behavior in $Fe^{3+}(Fe^{2+}Fe^{3+})O_4$ ceramics as a result of electron hopping between $Fe^{2+}$ and $Fe^{3+}$ in the octahedral sites. This mechanism was adopted to explain not only the electrical behavior of $Fe_3O_4$, but also the variations observed in solid solutions with insulating spinels and perovskites. In the small polaron model, electrical conductivity occurs by the hopping of either electrons or holes. Earlier, this hopping process was empirically determined to occur between ions of the same species but of different valency, which are present on equivalent lattice crystallographic sites. Moreover, these ions must differ in valency by only one unit. In the case of spinels this occurs between ions in octahedral positions, because hopping distances for ions in tetrahedral sites are larger. More recently, some authors consider hopping between multivalent ions of different chemical species occupying octahedral positions,[50] for instance, $Mn^{+3}+Cu^{2+}+Mn^{4+} \Leftrightarrow Mn^{+4}+Cu^{+}+Mn^{4+}$ and $Mn^{+3}+Cu^{2+}+Mn^{4+} \Leftrightarrow Mn^{+4}+Cu^{2+}+Mn^{3+}$. On the other hand, stable trivalent ions such as $In^{3+}$ or $Al^{3+}$ can substitute for $Mn^{3+}$ to ensure an increase in the resistivity and, consequently, an increase of the *B*-values.[85] Oxygen partial pressure plays an important role in the concentrations of charge carriers and, consequently, electrical conductivity. This is because cooling from sintering is carried out in air, which results in the oxidation of ceramics, which in Kröger-Vink notation can be written as follows: $1/2O_2 \Leftrightarrow O_o^{\times} + 1/4V_A^{II} + 1/2V_B^{III} + 2p^{\bullet}$.

In ionic compounds, the mobility of electrons it is largely determined by their interactions with the polar modes. The electron induces a localized polarization and distortion of the lattice, which moves along with the electronic carrier. The lattice vibrations promote the charge transfer from a donor (e.g. $Mn^{4+}$) to an acceptor (e.g. $Mn^{3+}$). In this case, conductivity is given by

$$\sigma = c(1-c)\left(\frac{e^2a^2\nu}{kT}\right)\exp\left(-\frac{E_\mu}{kT}\right) \quad (4)$$

where $c$ and $(1-c)$ are the probability of having a $Mn^{3+}$ or $Mn^{4+}$ ion in an octahedral site, respectively, $E_\mu$ is the activation energy, ν is the phonon frequency ($\sim 10^{13}$ Hz), and a is the transport distance. Small polaron mobilities are reported to be on the order of $10^{-4}$–$10^{-2}$ cm$^2$/V·s.

Conclusive proof of small polaron conduction can be established from (i) an activated mobility and (ii) a temperature independent Seebeck coefficient at a fixed deviation from the stoichiometry.[83] In the latter case, the thermopower is given by

$$Q = \pm\left[\ln\beta\left(\frac{1-c}{c}\right) + \frac{S_T}{K}\right] \quad (5)$$

where β is the a degeneracy factor involving the spin and the orbital degeneracy of the electronic carrier and $S_T$ is the vibrational entropy associated with the polaron environment. The sign of $Q$ indicates if the conductivity is *p*- or *n*-type.[47]

When $Q$ is temperature independent, this indicates that the activation energy for conduction is therefore associated to

mobility. In contrast, the Seebeck coefficient for a broadband semiconductor is strongly dependent on temperature; however, the activation energy for conductivity is associated with carrier production and not with the mobility. Moreover, in this case, the activation energies for thermopower and conductivity are equivalent.[47]

Electrons in localized states in a disordered solid can also move by a phenomenon known as variable-range hopping (VRH). Recently, Schmidt *et al.*[86] suggested that the electrical resistivity in bulk ceramics and thick films are better described by a VRH model, given as $\rho \sim T^{2p}\exp(T_0/T)^p$, whereas the resistivity of thin-films is better described by a nearest-neighbor hopping mechanism, given by $\rho \sim T\exp(T_0/T)$.

The interrelationships between semiconduction, defect structure, and chemistry in NTCR ceramics are rather complex and in places imperfectly understood. This arises basically from the complexity and variety of phenomena occurring in transition-metal spinels, such as temperature dependence of inversion degree, decomposition, and the less-explored oxygen nonstoichiometry. In fact, the majority of work published about nickel manganate-based NTCR thermistors assumes that the samples are stoichiometric with respect to oxygen. This might not always be the case, so this assumption overlooks the possibility of a small oxygen nonstoichiometry contributing to the charge carriers present. This is definitely an area that deserves further investigation.

*(C) Electrical Microstructure:* The electrical microstructure of NTCR ceramics has also been characterized by means of AC impedance spectroscopy. Contradictory reports can be found in the literature. For example, Irvine *et al.*[87] modeled the electrical response of $(Ni_{0.36}Zn_{0.64})_{1-x}Fe_{2+x}O_4$ ceramics with an equivalent circuit consisting of two parallel RC components in series, corresponding to grain boundary and bulk responses. They observed these electroactive regions to exhibit remarkably distinct temperature dependences. The grain boundary contribution, which is much larger, appears to be sensitive to annealing conditions, even at quite a low temperature (<200°C). Ferreira *et al.*[88] investigating $Co_xFe_{3-x}O_4$ ceramics, also evidenced the presence of bulk and grain boundary electroactive regions. Because the activation energy for the grain boundary and bulk showed similar values, they concluded that the conduction in these regions should have the same origin. Nevertheless, they observed a sudden increase in the activation energy at $x = 1$, which they ascribed to an *n*- to *p*-type conductivity transition. More recently, Song *et al.*[89] provided a different picture for the interpretation of the electrical response of MnCoCuO NTCR ceramics. Although they observed two relaxations, they ruled out a grain boundary response. Instead, they suggested the existence of two distinctive types of grains, which are either Cu-poor or Cu-rich. In 2004, Lee *et al.*[90] carried out microcontact impedance spectroscopy on $Mn_{0.476}Zn_{0.468}Fe_{2.056}O_4$ ceramics. They concluded that the resistance of the grain boundaries depends on their degree of oxidation, which ultimately is associated to the degree of misorientation of the grain boundaries. Probably, it should be contemplated that sintering NTCR ceramics in oxidizing atmospheres may lead to the existence of a *p*-type semiconductor at or near the grain boundaries, which gradually turns into an *n*-type in the grains interior, with all the consequences in the conduction processes that this would entail. To my knowledge, this premise was never analyzed but certainly deserves consideration.

*(D) Voltage/Current Characteristics:* The voltage/current characteristics of any NTCR thermistor show three regimes, as illustrated in Fig. 7. In the first regime, the voltage and current are directly proportional to each other ($dV/dI = R$ = constant). The resistance value is uniquely determined by the ambient temperature. In fact, this is the operational regime of temperature sensors. This is followed by a nonlinear regime, where at the maximum voltage, a decrease in resistance occurs as a result of the effects of self-heating. The relative decrease in resistance is equal to the relative increase in current ($dV/dI = R$ = constant). Finally, a third regime begins when the decrease in resistance is greater than the increase in current ($dV/dI < 0$). This is the operational regime for inrush current limiters and liquid level sensors.

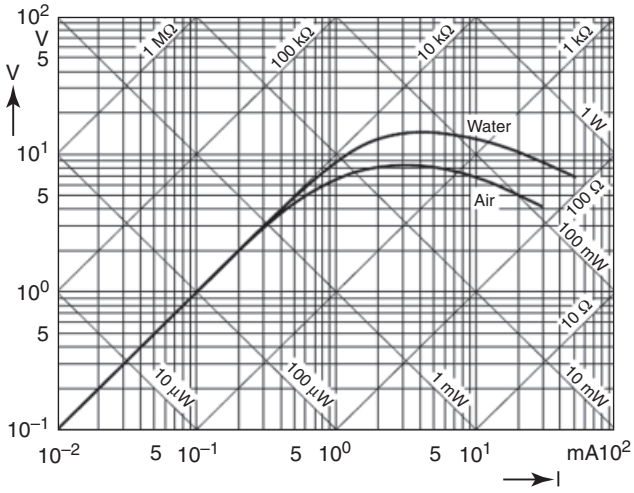


**Fig. 7.** Typical voltage current characteristics of NTCR thermistors. NTCR, negative temperature coefficient of resistance. (Courtesy from EPCOS AG, Germany)

### *(2) Thermal Properties of NTCR Thermistors*

It was already mentioned that self-heating of a NTCR thermistor occurs when current passes through it. This effect depends not only on the applied power, but also on the thermal dissipation factor, $\delta_{th}$, and the geometry of the thermistor itself. $\delta_{th}$ is given by $\delta_{th} = dP/dT$, i.e. the ratio in power dissipation and the resultant change in the thermistor's body temperature. Basically, it measures the power load required to increase the body temperature by 1 K. In general, $\delta_{th}$ for disk, rings (Fig. 2(a)), and surface-mounted device (SMD) components (Fig. 2(f)) mounted on printed circuit boards varies from 2.5 to 3.5 mW/K, whereas for glass-encapsulated thermistors (Fig. 2(d)) it ranges from 0.4 to 1.5 mW/K. Inrush current limiters (Fig. 2(b)) show larger $\delta_{th}$, which may reach 30 mW/K.

The heat capacity, $C_{th}$, which corresponds to the amount of heat (mJ/K) necessary to increase the body temperature by 1 K, is given by $C_{th} = \Delta H/\Delta T$. In general, $C_{th}$ varies from 1.5–2 mJ/K for a glass-encapsulated thermistor (Fig. 2(d)) to 3900 mJ/K for an inrush current limiter (Fig. 2(b)).

On the other hand, the so-called thermal cooling time constant, $\tau_c$, is expressed by $\tau_c = C_{th}/\delta_{th}$. This amount refers to the time required for an unloaded NTCR thermistor to vary its temperature by 63.2% of the temperature difference between its mean temperature and the environment temperature, under negligible power dissipation conditions. $\tau_c$ depends to large extent on the component design. In practice, $\tau_c$ values vary from 1 s for a bead thermistor, 15–30 s for disc and small rod thermistors, to 200 s for a disc encapsulated in a molded resin case.

### *(3) Aging of the Electrical Characteristics of NTCR Ceramics*

The change of the electrical properties with respect to time is generally referred to as aging. Unfortunately, this time dependent phenomenon affects nearly all passive electronic components (capacitors, piezoelectric, and NTCR temperature sensors) and leads to their eventual failure under service. Aging in NTCR ceramics manifests itself through a noticeable time dependence of both total resistance and sensitivity, which becomes ultimately reflected as a thermometric drift. Apparently, this phenomenon affects all NTCR ceramics to a more or less extent, independent of their composition.

Historically, aging of the electrical characteristics of NTCR ceramics was first reported in detail by Becker *et al.*[7] in 1946. Back then, these workers observed an almost exponential

increase in electrical resistance with time. They observed this resistance drift to be more dramatic during the first day of isothermal exposure and to gradually stabilize after 500 to 1000 h. They postulated that in order to obtain a stable thermistor, it was absolutely necessary to (1) select only semiconductors which are pure electronic conductors, (2) select those which do not change chemically when exposed to the atmosphere at elevated temperatures, (3) select a semiconductor that is not sensitive to impurities likely to be encountered during manufacture or use, (4) treat the material in order to reach chemical equilibrium of the impurities, that equilibrium is very sluggish during operation, (5) make a contact that is intimate, sticks tenaciously, has an coefficient of thermal expansion compatible with that of the semiconductor, and is durable in the atmospheres to which it will be exposed, (6) encapsulate the semiconductor with a glass or material that is impervious to gases and liquids, and finally, (7) preage the component for several days or even weeks at a temperature somewhat higher than that to which it will be subjected. In principle, remarkably improved resistance stabilities can be attained by observing these seven almost "sacred" precautions.

In 1978, Wood *et al.*[91] from the National Bureau of Standards (now NIST) collected disk and glass bead thermistors from six different manufacturers (Fenwal Electronics, Inc., Framingham, MA; Gulton Industries, Inc., Metuchen, NJ; Keystone Carbon Company, St. Marys, PA; Thermometrics, Inc., Edison, NJ; Victory Engineering Corporation, Springfield, NJ; and Yellow Springs Instrument Company, Yellow Springs, OH) and investigated their stability at 0°, 30°, and 60°C over a period of 2 years. Among their many observations and conclusions, they noted (1) the drift rate for beads and disks was fairly uniform for each manufacturer, (2) glass bead thermistors were more stable than their disk counterparts, (3) stability decreased with increasing temperatures, and (4), in particular, the drift rate of glass bead thermistors was virtually independent of both aging temperature and the initial resistance of the thermistor. Finally, they reported mean drift rates in the order of 0–2 mK over a 100-day-period. Later, the results of Wood *et al.*,[91] Edwards *et al.*[92] would corroborate Becker's sixth recommendation, that aging can be minimized through glass encapsulation. In fact, good quality glass bead thermistors can offer stabilities better than 0.5 mK per year, which makes them competitive with RTDs. None of the aforementioned works provided a clear insight into the origin(s) of aging in NTCR ceramics. This topic was first addressed in 1982 by Zurbuchen and Case,[93] who showed how different contributions to resistance drift from lead, solder, electrode, and interface could be determined from the change in the resistance versus temperature curves. For example, thermometric drift as a result of contact degradation should be larger at higher temperatures, whereas changes in the bulk properties should have the same thermometric drift, independent of the measuring temperature. Here, it should pointed out that a variation the B-constant should be expected in the case of pure thermometric drift because of changes in the ceramic characteristics, whereas a contact degradation should not cause any variation on the B-constant. They also proposed that once the contact degradation is minimized, thermometric drift as a result of bulk changes in $NiMn_2O_4$ thermistors could be caused by two mechanisms. One mechanism is the change of the crystal structure and the other is a nonequilibrium degree of inversion. These two parameters are strongly dependent on sintering conditions and cooling rates. These authors also suggested that firing of the silver electrodes at 700°C induces the typical equilibrium degree of inversion for that temperature. To a certain extent, this equilibrium persists on cooling. Hence, aging should be regarded as a tendency to reach the equilibrium state of inversion. At a low temperature, the degree of inversion in $NiMn_2O_4$ is greater; therefore, the concentration of $Mn^{3+}$ in octahedral sites is lower. Hence, the resistance should increase by this cation redistribution. These authors rejected oxidation-induced aging.

From the 1990s onwards there has been a considerable amount of research aimed at understanding aging in NTCR ceramics, as attested by a considerable number of publications in the literature.[50,85,93–103] Nevertheless, most investigators are still divided concerning the exact origin of the aging of the electrical properties of spinels; however, theories based on redistribution of charge over time are often evoked. This may occur by diffusion of cationic vacancies or changes in the degree of inversion. Basically, the first model is based on the preferential reoxidation of grain boundaries upon cooling from the sintering temperature, whereas the second is based on cation redistribution in spinels. Fritsch *et al.*[104] proposed a third mechanism that involves a possible combination of both cation redistribution and oxidation during high-temperature electroding.

Independent of the mechanism proposed to explain aging, it is commonly observed that quenched samples show lower levels of aging in comparison with slow-cooled samples,[95] as illustrated in Fig. 8(a). Aging is also dependent on composition, as shown for the Mn–Ni–Fe–O system[96] in Fig. 8(b).

According to the cation redistribution model, ageing is based in a decrease of "conducting paths" for conduction, i.e. the reduction of hopping pairs in the octahedral sites. For example, Castelan *et al.*[50,95] proposed in two distinct publications that aging in the $Mn_{7/3-x}Ni_{2/3}Cu_xO_4$ results either from $Cu^{2+}$ transfer from tetrahedral to octahedral sites or from $Ni^{2+}$ transfer from octahedral to tetrahedral. Independent to the question of which is the correct model, in both cases aging can be explained by a modification of the $[Mn^{3+}]/[Mn^{4+}]$ ratio. Fritsch *et al.*[104] demonstrated that cationic distribution in nickel manganite spinels is particularly sensitive to cooling rates; therefore, any metallization process involving heat treatment (normally at 800°–900°C) may affect this distribution ($Ni^{2+}$ transfer from octahedra to tetrahedra). They also observed the presence of "coffee bean"-like shape precipitates of ~20–40 nm in samples annealed at 850°C. They proposed that these precipitates resulted from oxidation. Upon aging, these precipitates disappear. Hence, aging was believed to result from reduction, through the diffusion of vacancies to the ceramics' surface. This assumption was supported by the virtual absence of aging under nitrogen. Metz[102] also suggested that aging is associated with the heat treatment used in the application of electrodes, which would

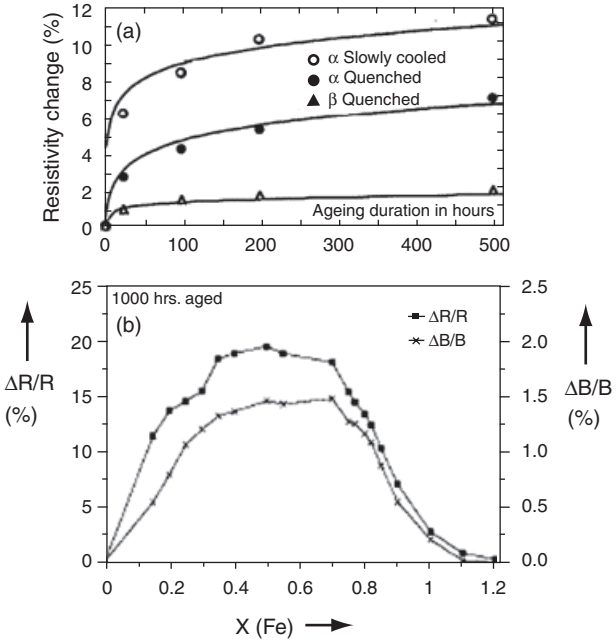


**Fig. 8.** (a) Typical resistance drift for quench and slow-cooled nickel-copper-manganese spinels (Reprinted with permission from Castelan *et al.*,[100] Copyright 1992, American Institute of Physics), and (b) compositional dependence of resistance and B-value drifts in slow-cooled $Mn_{2.46-x}Ni_{0.54}Fe_xO_4$ ceramics after 1000 h aging at 150°C. (With kind permission from Springer Science + Business Media: Groen *et al.*,[96] p. 81, figure 5)

promote $Mn^{3+}$ clusters. This should also account for the higher aging exhibited by tetragonal versus cubic spinels.

In 1999, Groen *et al.*[98] proposed aging to be associated with the oxidation of the grain boundaries. Their model is schematically illustrated in Fig. 9. Basically, if stoichiometry cooling or quenching are used, the reoxidation of the grain boundaries is suppressed. On slow cooling in air, reoxidation occurs preferentially at the grain boundaries, according to $1/2O_2 \Leftrightarrow O_o^{\times} + 1/4V_A^{II} + 1/2V_B^{III} + 2p^{\bullet}$. The cation vacancies formed at the grain boundaries will diffuse to the bulk at higher temperatures. This model was proposed based on magnetic measurements coupled with ac impedance and Seebeck measurements.[98] Both vacancies will occupy their thermodynamically favorable site, which will result in electrical drifts. In general, cationic vacancies diffuse preferably to the B-sites inside the grains. This increase B-site vacancies inside the grains results in an increase of resistivity, because the conduction in these materials occurs by electron or hole hopping over the B-sites.[96]

The cation redistribution model has been recently evoked by Wang *et al.*[105] to explain aging in $Fe_xMn_{2.34-x}Ni_{0.66}O_4$ ($0<x<1$) ceramics. These authors proposed the migration of $Fe^{3+}$ from octahedra to tetrahedra. The same authors investigated the effects of $O_2$ and $N_2$ annealing on the aging of $Fe_{0.5}Mn_{1.84}Ni_{0.66}O_4$.[101] Their observations were in agreement with Groen's model.

In 2000, Metzmacher *et al.*[85] proposed that the large volume wall associated with a fine-scale tweed grain submicrostructure may reduce aging by ferroelastic pinning $Mn^{3+}$, inhibiting charge redistribution between tetrahedra and octahedra. The cation redistribution model to explain aging in spinels is also indirectly supported by the higher stability exhibited by perovskite-based NTCR thermistors, where A to B cation transitions are rather improbable.

The effect of compositional purity on aging was also examined by several investigators, and their results are contradictory. For example, Gyorgyfalva *et al.*[106] observed that single-phase materials exhibit less aging, whereas Vakiv *et al.*[107] and Shpotyuk *et al.*[99] believed that aging is substantially eliminated by the presence of a small concentration of a NiO-based secondary phase. Several procedures have been strategically implemented to circumvent aging in commercial NTCR ceramics. This phenomenon has been successfully minimized by compositional manipulation,[50,95,100,108–111] glass encapsulation, and preaging treatments; however, its interpretation remains a controversial matter despite intensive research worldwide.

## V. Processing and Design of NTCR Devices

Despite the large variety in shapes, sizes, and electrical specifications, the industrial production of NTCR thermistor components has been accomplished by conventional ceramic technology. In fact, the preparation of NTCR devices still has more in common with the preparation of traditional whitewares than it has with the manufacture of other groups of semiconductors used in the electronic industry. Nonetheless, mass production and tight tolerance requirements also demanded some innovative machinery and complex processes, especially for the manufacture of glass-encapsulated thermistors and SMDs. Although much information concerning to relationships between the stability of devices and composition remains unavailable to the public because of proprietary reasons, general principles on processing are available in the technical handbooks of most manufacturers. Prior to the presentation of these general principles, the importance of phase diagrams in materials processing is discussed from an industrial viewpoint.

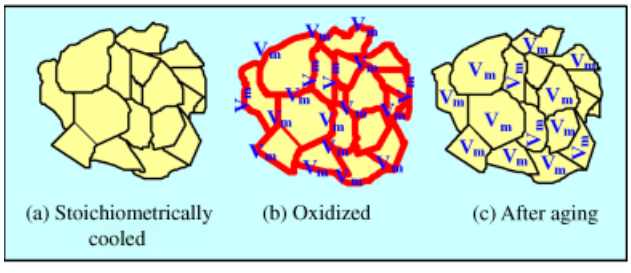


**Fig. 9.** Schematic model for aging in NTCR ceramics. (Adapted from Groen *et al.*[96]). NTCR, negative temperature coefficient of resistance.

### *(1) Phase Diagrams*

Phase diagrams can be regarded as "road maps" for materials processing, as they provide the necessary information for the preparation of high quality single-phase materials. For example, the preparation of single-phase stoichiometric $NiMn_2O_4$ from pure oxides is rather difficult. The reaction below 940°C, between $Mn_2O_3$ and refractory NiO, proceeds very slowly. However, if the temperature is raised too soon, $Mn_2O_3$ is converted to $Mn_3O_4$ (with the tetragonal spinel structure). The successful synthesis of $NiMn_2O_4$ depends therefore on processing this material within a narrow temperature range.[33] A comprehensive phase diagram for the Ni–Mn–O system in the temperature range 500°–1200°C was given by Wickham,[33] as illustrated in Fig. 10. According to this phase diagram, $NiMn_2O_4$ ($R = 0.667$) is stable in air between 750° and 900°C. Below 750°C, $NiMn_2O_4$ decomposes according to $2\ NiMn_2O_4 + 1/2\ O_2 \leftrightarrow \alpha Mn_2O_3 + 2\ NiMnO_3$. Above 900°C, it decomposes according to $Ni\ Mn_2O_4 \leftrightarrow x\ \ NiO + x/6O_2 + (3-x)/3Ni_{(3-3x)/(3-x)}Mn_{(2x)/(3-x)}Mn_2O_4$. In $O_2$-rich atmospheres, this reaction is shifted to higher temperatures. Gyorgyfalva and Reaney[112] studied this reaction in detail, and observed that the decomposition resulted in a spinel phase and a rock salt structure phase, which contains spinel-structured precipitates, as illustrated in Fig. 11. They proposed the decomposition to be driven by the reduction of the degree of inversion, followed by $Mn^{3+}$ clustering. At the transition temperature, sufficient nickel is present in the A-site to promote the transformation from spinel to rock salt.

Feltz and Polzl[113] produced an interesting ternary phase diagram for the Fe–Ni–Mn system, showing a region for the formation of single-phase spinel and temperatures for decomposition, as illustrated in Fig. 12. In this region, it is observed that the lower the Ni content, the higher the decomposition temperature. These materials exhibit room-temperature resistivities ranging from 4.7 and 950 kΩ.cm, whereas the B-values vary from 3300 and 5000 K. Nevertheless, they are only usable below 400°C, because of aging effects. Abe *et al.*[114] also determined the formation region of single-phase spinel in Mn–Co–Ni between 700° and 1100°C. They observed this region to shrink with increasing temperatures. More recently, chemical combinatorial techniques were used to establish the "electrical landscape" in the $NiO–Mn_2O_3–CuO$ system, as illustrated in Fig. 13.[115] Although this technique provides a rapid method of

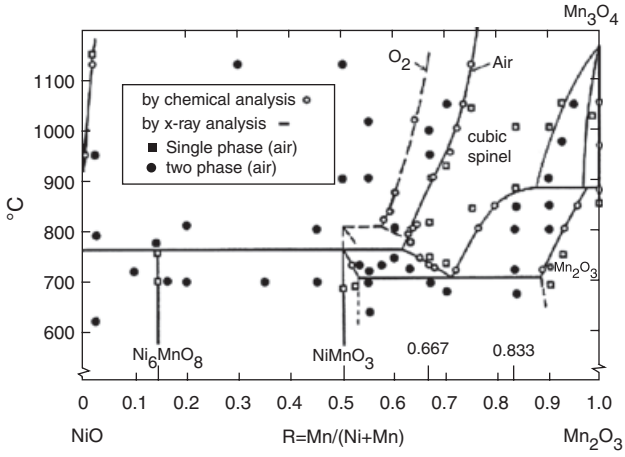


**Fig. 10.** Phase diagram for the Ni–Mn–O system. (Adapted from Wickham[33]).

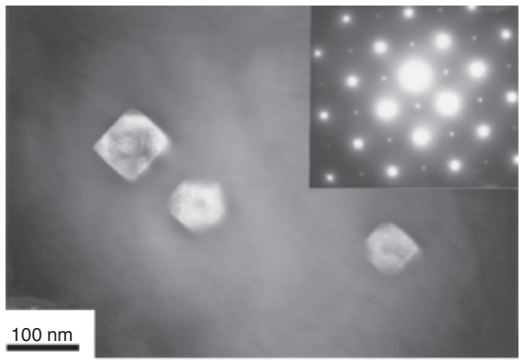


**Fig. 11.** TEM micrograph showing spinel precipitates in rock salt structure grains.[112] TEM, transmission electron microscopy. (Reprinted from de Gyorgyfalva and Reaney.[112] Copyright 2001, with permission from Elsevier.)

characterization, it is important to appreciate that in an industrial environment, a shift of properties and stability may occur due to processing and sintering cycles. Vakiv *et al.*[116] performed a similar study using samples prepared by the traditional ceramic technology.

### *(2) Powder Synthesis*

NTCR ceramic thermistors are traditionally manufactured from powders that are synthesized according to the mixed oxide route. Basically, two or more metal oxide powders such as manganese, iron, cobalt, nickel, copper, and zinc are ultimately mixed using conventional milling techniques (e.g. ball milling, attrition milling, etc.). This process is aimed not only at homogenizing the mixture but also at enhancing powder reactivity, due to particle size reduction. Subsequently, the desired phase or phase assemblages are synthesized by solid-state reaction at high temperatures. Both the purity and crystallinity of the products are routinely evaluated by powder X-ray diffraction. This quality control process is followed by a milling step for a reduction in particle size and increase in the specific surface area. These two variables are crucial for subsequent processes such as tape casting and sintering. Suitable organic binders, solvents, plasticizers, and surfactants are added to the powders at the final milling stage. In general, binders are used to improve the mechanical strength of the green bodies, so they can be easily manipulated before the firing process, but binders also promote the fabrication of low porosity, defect-free parts.

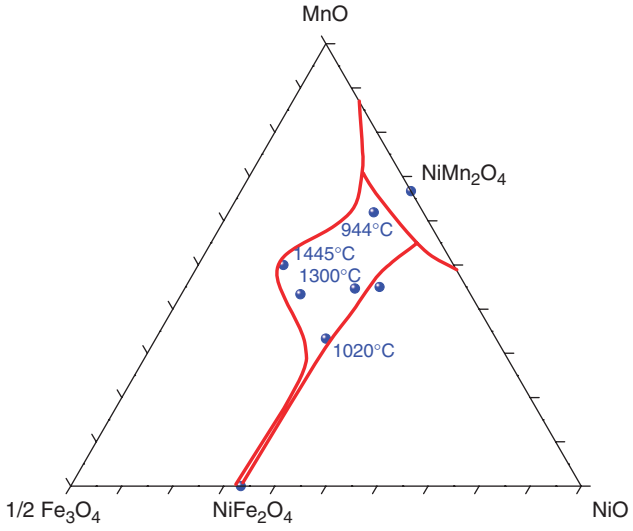


**Fig. 12.** Spinel formation area of the system $Fe_xNi_yMn_{3-x-y}O_4$ and temperature of decomposition from DTA measurement. (Adapted from Feltz and Polzl[113]).

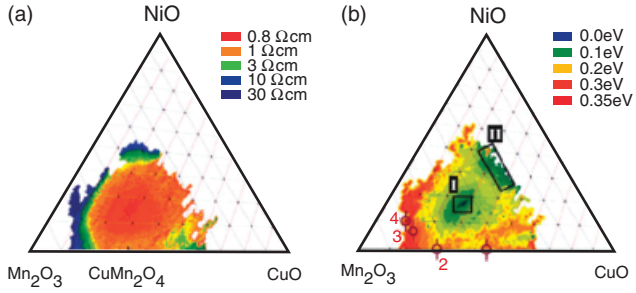


**Fig. 13.** (a) Conductivity map taken at 25°C, and (b) activation energy of the thermally activated conduction for the $Mn_2O_3$–CuO–NiO composition spread-film. Compositions one to four have standardized thermistor characteristics. Areas I and II have low temperature dependences. (Reused with permission from D. A. Kukuruznyak *et al.*,[115] Copyright 2005, American Institute of Physics).

A number of alternative routes have been proposed to overcome the aforementioned difficulties encountered during the synthesis of transition-metal oxide spinels in the $Ni_{1-x}M_yMn_{2+x-y}O_4$ (M = Co, Ni, Fe, Cu) systems. Chemical routes were favored by many researchers,[59,117] because they provide a relatively easy route to synthesizing single-phase powders of controlled stoichiometry. The most popular chemical route for the preparation of spinels is the coprecipitation of metal oxalates ($M \cdot C_2O_4 \cdot 2H_2O$) from metal chlorides in an oxalate solution, as originally proposed by Wickham.[33] Other techniques include the precipitation of nickel nitrate and manganous oxalate under alkaline conditions.

Recently, Wang *et al.*[118] synthesized $NiCo_{0.2}Mn_{1.8}O_4$ nanopowders via an auto-combustion process of nitrate–citrate gels. This combustion process of the dried gel can be divided into two steps. The first step is the decomposition and auto-combustion of the gel, which occurs at ~200°C. The second step is the combustion and decomposition of remnant carboxylate at ~290°C. After calcination at 800°C, a single-phase spinel is formed. This powder appeared to exhibit high sinterability, with fired ceramics reaching 97% of relative density.

### *(3) Forming and Firing*

The two most common forming methods used in the industry are pressing and tape casting. For example, components (a), (b) and (c) in Fig. 2 are formed by uniaxial dry pressing of spray dried powders, whereas components (d) and (f) are made from ceramic tapes. In certain situations, extrusion is also used as a forming method.

High-output rotative presses comprising hardened steel or carbide dies are used to shape disk and ring-shaped bodies. Superior compaction uniformity is achieved when spray dried powders are used. Free-flowing granules are then produced from slurry suspensions by flash evaporation in a hot circulating gas environment. Continuous tape casting machines are used for fabricating thick ceramic films. Prior to tape casting, the precursor slurry is deaired, in order to reduce posterior defects on the ceramic tape. After tape casting, the ceramic film is dried, blanked, and stored for sintering.

The initial stage of heat treatment concerns binder removal from the green body. Slow heating is often required for this process, in order to prevent warping, cracking, bloating, or particle rearrangements. A cooling rate that minimizes thermal shock stresses should also be chosen. In principle, thermal stress depends on the material and the dimensions of the component. Mechanical stress during manufacturing can induce microcracks, and their propagation under operation results in discontinuous drifts in resistivity.

The sintering temperature depends essentially on the chemical composition and the physical characteristics of the powder. In principle, NTCR ceramics exhibit better electrical performance when prepared as single-phase dense bodies; however, full dens-

ification is difficult to achieve when fabricating devices because of the sintering inertia imparted by the low firing temperatures used. The intentional formation of small amounts of liquid is often used to overcome this difficulty. Most NTCR manufacturers attempt to hold linear shrinkage in the range 15%–18%, for accurate dimensional control. Frequently, the upper limit of thermal stability of the spinel structure has to be exceeded during the sintering process, which leads to decomposition of the material, as previously described. Hence, annealing at temperatures within the stability limit of the spinel is invariably used to foment its recrystalization. On the other hand, electrodes are also often cofired with the ceramic; however, metallization can also be applied latter. Electrode integrity is evaluated by pulling test wires soldered to the electrodes. Poorly sintered electrodes tend to be porous and absorb fluxing agents during glass encapsulation. Overfired silver electrodes show weak contact/ceramic strength and give rise to high contact resistances. Hence, appropriate control of electroding and heat treatments are crucial in the industrial production of NTCR thermistors.

#### *(4) Manufacture of Glass-Encapsulated and Surface-Mounted (SMD) NTCR Sensors*

Most innovations in the field of thermistor fabrication concern the development of more accurate and stable components through compositional modifications. Nevertheless, there has been also a trend towards miniaturization. Miniaturized glass-encapsulated and SMD thermistors are fabricated using ceramic multilayer technology. The fabrication of multilayered SMD thermistors is basically accomplished by the same technological principles used for the manufacture MLCCs. Hence, green tapes are electroded by screen-printing, laminated, and subsequently cofired. The materials for inner electrodes are alloys of silver and palladium.

Most NTCR manufacturers use well-established metal ink formulations offered by metallic paste producers. In high reliability applications, gold can be used to avoid problems associated with silver migration under voltage stress.

Glass-encapsulated thermistors are fabricated from ceramic substrates, which were made by the lamination of several layers of ceramic tapes. These substrates can be cofired with electrodes printed on their faces or, alternatively, electroding can be performed as a postfiring step. The choice of process depends on the ceramic material. The electroded substrate is then cut to the required dimensions, using dicing or ultrasonic drilling equipment. These smaller parts are often refered to as wafers. A metallic paste is applied to the wafer's surface for the lead wire attachment. Cu-coated NiFe lead wires are often used so that they can be magnetically handled on a continuous production line. The contact paste is then hardened by a swift heat treatment, as illustrated in Fig. 14. This is followed by placing a short length of glass tube that completely covers the wafer and partially covers the electrical leads coming out of it. This glass is then heat treated near its softening point, in order to collapse over the ceramic/leads assembly, forming a bubble-free encapsulation. Sealing glass compositions should exhibit a good thermal expansion match and minimal chemical reaction. Low alkali glasses are often used to seal elements that operate up to 300°C; however, their use in sensors operating up to 500°C are ruled out, because the diffusion of alkali ions into the ceramic sensor alter its electrical properties.

Careful design of glass-encapsulated sensors and SMDs is required to minimize the stresses induced during assembly and subsequent thermal excursions. Particular attention should be given to thermal expansion mismatch of materials and stress relief at interfaces.

#### *(5) Thin-Film NTCR Sensors*

Although NTCR sensors are traditionally fabricated from high oxides via solid-state reactions at temperatures of around 1200°–1300°C, a growing demand for thin-film thermistors, especially for space and environmental applications, has led to several NTCR film deposition studies. For instance, very fast and rugged thermometers are desired for measurements of millimeter-scale turbulence in ocean waters.[119] Both surface topology and density are often regarded as the most important features controlling the performance and stability of NTCR thin-film sensors. Low porosity is desirable for minimizing deleterious effects arising from humidity or oxygen partial pressure changes, which may affect the sensor's performance by altering its electrical resistance. High-density films also impart better mechanical stability to the device.

**Fig. 14.** Manufacture of glass-encapsulated sensors. (Courtesy from EPCOS AG, Germany).

In 1998, Parlak *et al.*[120] unveiled the potential of electron beam evaporation (EBE) techniques for fabricating $NiMn_2O_4$ films exhibiting NTCR behavior. In 2004, Basu *et al.*[121] observed that $Ni_xMn_{3-x}O_4$ $(0.4 \leq x \leq 1)$ films deposited by RF sputtering exhibit an electrically inhomogeneous surface, with regions showing metallic behavior and others semiconductivity. Although homogeneity could be improved by annealing at 800°C, some regions showing metallic behavior persisted. Non-stoichiometry induced during deposition is believed to be responsible for these inhomogeneities. Schmidt *et al.*[122] compared the processability and the electrical characteristics of $NiMn_2O_4$ films fabricated by different deposition methods, including RF sputtering, EBE and screen printing.

In general, the sputtering targets used for RF sputtering or pulse laser deposition are obtained by the traditional ceramic processing described above. In order to ensure the target's mechanical stability during argon bombardment and reduce potential charge carrier leakage paths, the ceramic targets should exhibit high density. EBE it is a rather simple technique, which makes it favorable over other thin-film deposition processes such as RF sputtering. In EBE, the source powder can be of any average particle size and/or particle size distribution and needs no further processing. The deposition process often does not require a specific gas atmosphere, and the deposition rate can be varied easily by adjusting the beam current. In both techniques, after deposition, the films usually require annealing at high temperatures. The major shortcoming of these techniques concerns the difficulty in controlling the stoichiometry.

## VI. Applications of Thermistors

The largest share of thermistors (~40%) is used in automobiles, whereas consumer electronics account for another 30%. The use of NTCR thermistors in medical applications has been gradually gaining expression. The applications of NTCR ceramics are generally divided into the following categories: (1) zero power sensing applications, which rely on the temperature dependence of resistance, and (2) self-heated applications, which take advantage of the voltage–current characteristics of NTCR thermistors. Temperature measurement is the most common application for NTCR ceramics, and a few examples are given below.

### (1) Automotive Temperature Monitoring

Since the late 1940s, NTCR thermistors have been used in automotive applications to send signals to gauges and, more recently, to electronic control modules. The ever-increasing trend towards improved automobile performance in terms of drivers' comfort and safety, results in more complex systems. Invariably, new systems demand a larger number and variety of temperature sensors, which simultaneously should obey more stringent requirements, such as operation at extreme conditions of temperature. The most common applications of NTCR thermistors in automobiles are as follows: temperature measurement of cooling water and oil, temperature monitoring of exhaust gas, cylinder head or braking system, and controlling the air conditioning system. The use of NTCR thermistors in the air conditioning system of an automobile is schematically illustrated in Fig. 15.

The control of any air conditioning system should involve the least possible intervention from the driver, so he can focus on the road. NTCR sensors are at the heart of this level of automation. For example, NTCR 1, the so-called evaporator sensor, plays a crucial role in air conditioning systems. It controls the temperature of the evaporator, whereas NTCR 2 ensures that moisture does not freeze on the evaporator, blocking the air stream. NTCR 4 and 5 are the internal and external temperature sensors, respectively. In conjunction with NTCR 6, which measures the temperature of the blown air on each air outlet (e.g. towards feet), and NTCR 3, which measures the temperature of mixed air, these sensors ensure more efficient air conditioning systems. Better efficiencies reduce both fuel costs and exhaust emissions, complying with emerging environmental legislation.

### (2) House Appliances

NTCR thermistors are suitable for temperature measurement in a large variety of household appliances, such as washing machines, refrigerators, electric cookers, hair driers, coffee makers, electric kettles, etc. They are also used in building automation controls (e.g. fire alarms), home heating, and air conditioning systems. The intensified market competition leads to more sophisticated products, a trend that is followed by household appliances and will result in a natural demand for NTCR thermistors. The use of NTCR thermistors in a washing/drying machine is schematically illustrated in Fig. 16.

In this example, NTCR sensors are used to measure the temperature of the washing water (also corrosive medium as a result of soaps), the temperature of the inflow drying air, and vented air. In order to optimize anti-wrinkling, a temperature sensor can be integrated in the steam generator.

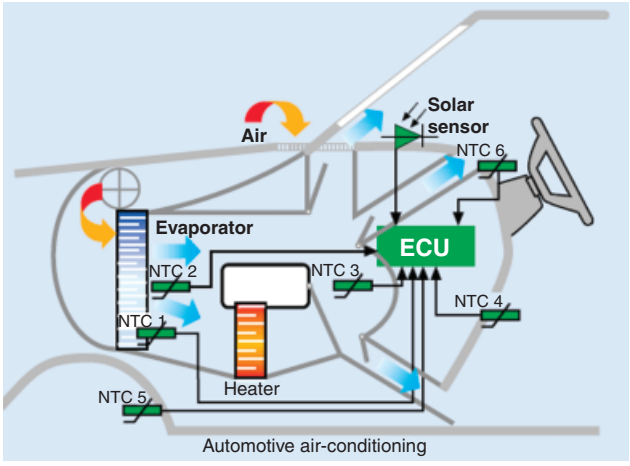


**Fig. 15.** Examples of NTCR sensors found in air conditioning. NTCR 1: evaporator sensor, NTCR 2: Evaporator air sensor, NTCR 3: air mix sensor, NTCR 4: interior temperature sensor, NTCR 5: external temperature sensor, and NTCR 6: air outlet sensor. (Courtesy: EPCOS AG, Germany). NTCR, negative temperature coefficient of resistance.

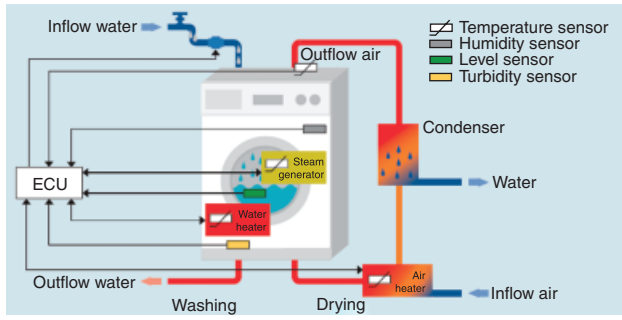


**Fig. 16.** Examples of NTCR sensors found in washing/drying machines. (Courtesy: EPCOS AG, Germany).NTCR, negative temperature coefficient of resistance.

### (3) Healthcare

NTCR thermistors are finding an increasing number of applications in medical procedures. For example, during hemodialysis, blood is removed from the patient's body, artificially filtered, and returned to the patient. NTCR thermistors ensure that the blood is then reheated to body temperature, before it is returned to the patient. Disposable thermometers based on NTCR components have been replacing mercury glass thermometers (typical response time 60–120 s), as the most widely used method for measuring human body temperature. These NTCR-based thermometers are characterized by an accuracy as high as $\pm 0.1$ K and by a short response time of 7 s, which allows a fast and simple measurement of a patient's body temperature. NTCR-based reusable thermometers for long-term measurements have also been developed. They are used for continuous monitoring of the patient's body temperature during induced hypothermia and general anesthesia procedures. They are also used to continuously measure the body temperature of infants in incubators. They are characterized by their great accuracy, rugged design, and high resistance to sterilization cycles. In fact, they feature an operating life of more than 100 sterilization cycles at 121°C for 20 min or at 134°C for 4 min. These reusable temperature probes are normally housed in plastic or metal shafts. Disposable hypodermic needle sensors are especially critical during open-heart surgery, when they are inserted into the myocardium muscle to monitor temperature. A hypodermic needle with a small NTCR thermistor can be inserted into targeted anatomical sites for temperature measurement and are well-suited for cancer research and treatment, particularly for brain tumors.

### (4) Other Applications

Surface-mounted NTCR thermistors, such those illustrated in Fig. 2, are used for temperature sensing and/or temperature compensation in: (i) Battery packages and battery chargers found in communication equipment, portable consumer electronics, audio and video equipment, power tools, and medical devices. In these applications, NTCR thermistors not only enable quicker charging times, but also ensure a better performance and life-time of the batteries. (ii) Liquid crystal displays (LCDs) found in mobile phones, autoradios, digital cameras, palm tops. NTCR thermistors automatically cancel temperature effects on LCD contrast, i.e. they maintain a constant contrast over a wide temperature range. Basically, they provide a stable voltage output despite variations in temperature.

The reliability of modern hard disk drives is strongly dependent on temperature. In fact, their effectiveness decreases with increasing temperature, and loss of data may occur at high temperatures. In order to prevent such a disastrous occurrence, SMD thermistors are then used for temperature monitoring. Hence, when the temperature exceeds the configuration limits (usually 55°C), NTCR thermistors trigger one of the following possible actions: activation of a cooling fan, slow-down of drive activity, or even stopping the drive.

Another application of NTCR thermistors is in liquid level sensors. This application relies on the voltage/current characteristics of thermistors. The temperature of an electrically loaded thermistor depends on the surrounding medium. Hence, when a thermistor is immersed in a liquid, the dissipation factor increases, the temperature decreases, and a voltage across the NTCR is established. Owing to this effect, thermistors are able to sense the presence or absence of liquids. In summary, NTCR thermistors promote more secure and optimized processes occurring within modern equipment.

## VII. Future Prospects

New combinations of electrical properties and physical dimensions are being developed by different manufacturers to meet the ever-increasing requirements set by the user's industries. This last section reflects first on the demands for NTCR ceramics for applications under extreme conditions and then on the technological challenges in terms of device fabrication. The author expresses his views in terms of exploring "novel" materials, based on slightly more complex structures than spinels and cubic perovskites.

### *(1) Development NTCR Sensors Operating Under Extreme Conditions*

There is an increasing need for sensors capable of operating at extreme conditions, in particular at high temperatures (near 1000°C or above). In the aerospace industry, for example, there is a growing need for gas turbines to operate at higher temperatures for higher operational efficiency with reduced emissions. This requires the application of high-temperature sensors (>1000°C) capable of accurate and reliable monitoring and control of the turbine's temperature. Also, the increased need for *in situ* monitoring of potentially hazardous gases (e.g. CO, $CO_2$, $NO_x$, volatile organic compounds (VOCs), and unburned hydrocarbons) has stimulated considerable activity in the development of NTCR thermistors. It is well known that measuring the temperature of corrosive liquids leads to life-shorting of temperature sensors. Hence, there is a need to develop suitable sensor housing.

### *(2) Device Fabrication*

Low temperature cofired ceramics (LTCC) technology is now well established at industrial levels, particularly in the field of wireless communication components. This technology enables successful 3D integration of electronic passive components. The further implementation of LTCC into new electronic applications motivates the research towards novel low firing materials that are cofirable not only with metals but also with other functional ceramics such as microwave resonators, ferroelectrics, piezoelectrics, and magnetics. Obviously, NTCR ceramics can also be incorporated into LTCC modules, for temperature compensation and voltage control.

Lately, substantial research has been conducted in the field of microfluidic devices. The integration of NTCR thermistors in microfluidic devices is certainly a direction to explore. Potential applications are in microsystems that handle cells and blood, which require a continuous and accurate control of temperature. Other applications in which control of temperature is crucial include microchemical systems dealing with polymerase and enzyme reactions. Spark plasma sintering should be explored for the densification of very refractory ceramics as an alternative to conventional pressureless sintering. Finally, electrophoretic deposition of ceramics is becoming a mature technique at the academic research level. Transfer of this technique to the industrial level will promote the fabrication of good quality ceramic films with controllable thickness and shape, which will make current postfiring shaping stages redundant.

### *(3) Exploring NTCR Behavior in "Novel" Materials*

Recently, Miranda and colleagues[123,124] has shown that, not surprisingly, many transition-metal based hexagonal perovskites show semiconductivity. Moreover, they also observed that the activation energy for conductivity in hexagonal perovskites appears to correlate to the relative number of face- and corner-shared octahedra and oxygen deficiency. Hence, the control of the electrical properties through a "*crystal-structure engineering*" approach may provide a "novel" method for tailoring sensitivity in NTCR ceramics. This approach also deserves consideration, for example, in layered compounds such as Aurivilius and Ruddlesden-Popper phases. Ruddlesden-Popper phases and can also be expressed by the general formula $AO(ABO_3)_n$, where AO represents a layer of rock salt structure (like the semiconducting NiO) separating n blocks of perovskite ($ABO_3$). In both families, the electrical characteristics (resistivity and activation energy for conduction) can possibly be controlled in a systematic fashion through the number of perovskite blocks in the structure and their electrical nature. Finally, compounds that are isostructural with the very popular[125,126] $CaCu_3Ti_4O_{12}$ may offer interesting properties for the development of NTCR ceramics. This heavily distorted perovskite shows semiconductivity by electron hopping between $Cu^{2+}$ and $Cu^{3+}$, a necessary condition for NTCR behavior. In this case, the activation energy for conduction may be tuned by changing the distortion in the structure, through chemical substitution doping on both the A-site and the B-site, whereas the level of conductivity might be controlled by minor additional doping (e.g. manganese).[127]

## Acknowledgments

The author would like to thank Drs. D. Orosel and D. Neuber from EPCOS for stimulating discussions. Dr. C. Hoffman, director of the Corporate Materials & Research Development, and Mr. Kloiber from the Sensors Department at EPCOS are also acknowledged for providing material for this review. Profs. Derek Sinclair and Ian Reaney from Sheffield University are also acknowledged for sharing their experience in the field of NCTR thermistors. Thanks also go to Prof. Feltz for the same reasons. I would like to thank Mrs. Penzinger and Cebular from the EPCOS OHG Powder Laboratory for sharing their experience in ceramic processing. Finally, I would like to thank EPCOS AG, Germany for supplying figures for this work.

## References

[1]T. D. McGee, *Principles and Methods of Temperature Measurement*. Wiley-IEEE, New York, 1988.
[2]M. Faraday, "On Conducting Power Generally"; pp. 119–26 in *Experimental Researches in Electricity*. Royal Institution, London, 1833.
[3]S. Ruben, "Electrical Pyrometer Resistance"; U.S. Patent #2021491, 1930.
[4]P. G. Andres, "Method of Making Electrical Resistance Elements"; U.S. Patent #2027413, 1933.
[5]J. Amstel, "Electrical Resistance Material"; U.S. Patent #2111708, 1935.
[6]W. Schottky, "Thermonegative Resistor"; U.S. Patent #2183755, (1935).
[7]J. A. Becker, C. B. Green, and G. L. Pearson, "Properties and Uses of Thermistors—Thermally Sensitive Resistors," *Bell System Tech. J.*, **26** [1] 170–212 (1947).
[8]E. D. Macklen, *Thermistors*. Electrochemical Publications Ltd, Ayr, 1979.
[9]G. L. Pearson, "Resistance Device"; U.S. Patent #2276864, 1939.
[10]E. J. W. Verwey and M. G. van Bruggen, "Structure of Solid Solutions of $Fe_2O_3$ in $Mn_3O_4$," *Z. Kristallogr.*, **92** [1/2] 136–8 (1935).
[11]E. J. W. Verwey and J. H. De Boer, "Cation Arrangement in a Few Oxides with Crystal Structures of the Spinel Type," *R. Trav. Chim. Pays-Bas*, **55**, 531–40 (1936).
[12]J. H. De Boer and E. J. W. Verwey, "Semi-Conductors with Partially and with Completely Filled 3d-Lattice Bands," *Proc. Phys. Soc.*, **49**, A59–71 (1937).
[13]E. J. W. Verwey, "Electronic Conduction of Magnetite ($Fe_3O_4$) and its Transition Point at Low Temperatures," *Nature*, **144**, 327–8 (1939).
[14]E. J. W. Verwey and P. W. Haayman, "Electronic Conductivity and Transition Point of Magnetite ("$Fe_3O_4$")," *Physica*, **8**, 979–87 (1941).
[15]E. J. W. Verwey and E. L. Heilmann, "Physical Properties and Cation Arrangement of Oxides with Spinel Structures .1. Cation Arrangement in Spinels," *J. Chem. Phys.*, **15** [4] 174–80 (1947).
[16]E. J. Verwey, P. W. Haayman, and F. C. Romeijn, "Physical Properties and Cation Arrangement of Oxides with Spinel Structures .2. Electronic Conductivity," *J. Chem. Phys.*, **15** [4] 181–7 (1947).
[17]E. J. W. Verwey, F. Deboer, and J. H. Vansanten, "Cation Arrangement in Spinels," *J. Chem. Phys.*, **16** [12] 1091–2 (1948).
[18]E. J. W. Verwey, P. W. Haaijman, F. C. Romeijn, and G. W. Vanoosterhout, "Controlled-Valency Semiconductors," *Philips Res. Rep.*, **5** [3] 173–87 (1950).

[19]F. Deboer, J. H. Vansanten, and E. J. W. Verwey, "The Electrostatic Contribution to the Lattice Energy of Some Ordered Spinels," *J. Chem. Phys.*, **18** [8] 1032–4 (1950).
[20]J. Torok, "Thermistor"; U.S. Patent #2700720, 1943.
[21]F. C. Romeijn, "Physical and Crystallographical Properties of Some Spinels .3. Preparation and X-Ray Investigation of Some Spinels," *Philips Res. Rep.*, **8** [5] 321–42 (1953).
[22]J. B. Goodenough and A. L. Loeb, "Theory of Ionic Ordering, Crystal Distortion, and Magnetic Exchange Due to Covalent Forces in Spinels," *Phys. Rev.*, **98** [2] 391–408 (1955).
[23]J. B. Goodenough, "Theory of the Role of Covalence in the Perovskite-Type Manganites [La,M]$MnO_3$," *Phys. Rev.*, **100** [2] 564–73 (1955).
[24]J. B. Goodenough, D. G. Wickham, and W. J. Croft, "Some Ferrimagnetic Properties of the System $Li_xNi_{1-x}O$," *J. Appl. Phys.*, **29** [3] 382–3 (1958).
[25]J. B. Goodenough, D. G. Wickham, and W. J. Croft, "Some Magnetic and Crystallographic Properties of the System $Li_xNi_{1-2x}Ni_xO$," *J. Phys. Chem. Solids*, **5** [1–2] 107–16 (1958).
[26]J. B. Goodenough, "An Interpretation of the Magnetic Properties of the Perovskite-Type Mixed Crystals $La_{1-x}Sr_xCoO_3$-Lambda," *J. Phys. Chem. Solids*, **6** [2–3] 287–97 (1958).
[27]D. G. Wickham and J. B. Goodenough, "Suggestion Concerning Magnetic Interactions in Spinels," *Phys. Rev.*, **115** [5] 1156–8 (1959).
[28]A. Wold, J. B. Goodenough, E. Whipple, and R. J. Arnott, "Crystallographic Transitions in Several Chromium Spinel Systems," *J. Appl. Phys.*, **34** [4] 1085–6 (1963).
[29]D. B. Rogers, A. Wold, and J. B. Goodenough, "Electrical Conductivity in Spinel System $Co_{1-x}Li_xV_2O_4$," *J. Appl. Phys.*, **35** [3P2] 1069–70 (1964).
[30]P. K. Baltzer and J. G. White, "Crystallographic and Magnetic Studies of the System $(NiFe_2O_4)1\text{-}X+(NiMn_2O_4)X$," *J. Appl. Phys.*, **29** [3] 445–7 (1958).
[31]J. D. Dunitz and L. E. Orgel, "Electronic Properties of Transition-Metal Oxides .2. Cation Distribution Amongst Octahedral and Tetrahedral Sites," *J. Phys. Chem. Solids*, **3** [3–4] 318–23 (1957).
[32]J. D. Dunitz and L. E. Orgel, "Electronic Properties of Transition-Metal Oxides .1. Distortions from Cubic Symmetry," *J. Phys. Chem. Solids*, **3** [1–2] 20–9 (1957).
[33]D. G. Wickham, "Solid-Phase Equilibria in the System NiO–$Mn_2O_3$–$O_2$," *J. Inorg. Nucl. Chem.*, **26** [8] 1369–77 (1964).
[34]D. G. Wickham, "Chemical Composition of Spinels in System $Fe_3O_4$–$Mn_3O_4$," *J. Inorg. Nucl. Chem.*, **31** [2] 313–20 (1969).
[35]E. M. Logothetis, K. R. Laud, and J. K. Park, "Rare Earth or Yttrium, Transition Metal Oxide Thermistors"; U.S. Patent #4162631, 1977.
[36]T. Matsuoka, Y. Matsuo, and S. Hayakawa, "High Temperature Thermistor Composition"; U.S. Patent #4013592, 1976.
[37]Y. Matsuo and S. Hayakawa, "High Temperature Thermistor Composition"; U.S. Patent #3962145, 1974.
[38]U. Walter, "High Temperature Thermistor (NTC)"; U.S. Patent #4126583, 1977.
[39]K. E. Schubert, "Resistor Compositions Containing Pyrochlore-Related Oxides and Cadmium Oxide"; U.S. Patent #3560410, 1969.
[40]V. A. M. Brabers and R. E. Vandenberghe, "Ionic Order and Cation Valencies in Spinels $Cu_{1.5}Mn_{1.5}O_4$ and $CuGaMnO_4$," *Phys. Lett. A, A*, **44** [7] 493–4 (1973).
[41]R. E. Vandenberghe, G. Robbrecht, and V. A. M. Brabers, "Stability of Cubic Spinel Structure in System Cu–Mn–O," *Mater. Res. Bull.*, **8** [5] 571–9 (1973).
[42]J. Klerk and V. A. M. Brabers, "New Possibility to Study Kinetics of Cation Redistribution in Spinels," *Phys. Status Solidi a-Appl. Res.*, **23** [1] K107–11 (1974).
[43]R. E. Vandenberghe, G. G. Robbrecht, and V. A. M. Brabers, "Structure and Ionic Configuration of Oxidic Copper-Manganese Spinels ($Cu_xMn_{3-x}O_4$)," *Phys. Status Solidi a-Appl. Res.*, **34** [2] 583–92 (1976).
[44]V. A. M. Brabers and J. Klerk, "Infrared-Absorption Spectrum and Inversion Degree of Manganese Ferrite," *Solid State Commun.*, **14** [7] 613–5 (1974).
[45]V. A. M. Brabers and J. Klerk, "Dilatometric and X-Ray Study of Cation Distributions in Spinels," *Z. Kristallogr.*, **146** [1–3] 92–2 (1977).
[46]Y. Kawaguchi and T. Kineri, "Thermistor Materials and Elements"; U.S. Patent #4952902, 1989.
[47]S. E. Dorris and T. O. Mason, "Electrical-Properties and Cation Valencies in $Mn_3O_4$," *J. Am. Ceram. Soc.*, **71** [5] 379–85 (1988).
[48]E. D. Macklen, "Electrical-Conductivity and Cation Distribution in Nickel Manganite," *J. Phys. Chem. Solids*, **47** [11] 1073–9 (1986).
[49]E. Jabry, G. Boissier, A. Rousset, R. Carnet, and A. Lagrange, "Preparation of Semiconducting Ceramics (NTC Thermistors) by Chemical Method," *J. Phys.*, **47** [C-1] 843–7 (1986).
[50]P. Castelan, B. Ai, A. Loubiere, A. Rousset, and R. Legros, "Aging Study of Ntc Thermistors by Thermopower Measurements," *Sens. Actuat.-Phys.*, **33** [1–2] 119–22 (1992).
[51]J. Certo, C. S. Furtado, A. R. Ferreira, and J. M. Perdigao, "Alpha-$Fe_2O_3$ Ceramics as Negative Temperature-Coefficient Thermistors," *J. Eur. Ceram. Soc.*, **11** [5] 401–5 (1993).
[52]A. Rousset, A. Lagrange, M. Brieu, J. J. Couderc, and R. Legros, "Influence of the Microstructure on Electrical Stability of NTC Thermistors," *J. Phys. Iii*, **3** [4] 833–45 (1993).
[53]Y. D. Hao, L. J. Chen, H. Lin, D. X. Zhou, and S. P. Gong, "Research on NTC Thermally Sensitive Powder Materials for Thick-Film Thermistors," *Sens. Actuat. a-Phys.*, **35** [3] 269–72 (1993).
[54]J. G. Fagan and V. R. W. Amarakoon, "Reliability and Reproducibility of Ceramic Sensors .1. NTC Thermistors," *Am. Ceram. Soc. Bull.*, **72** [1] 70–9 (1993).
[55]P. Fau, J. P. Bonino, J. J. Demai, and A. Rousset, "Thin-Films of Nickel Manganese Oxide for NTC Thermistor Applications," *Appl. Surf. Sci.*, **65–6**, 319–24 (1993).
[56]A. Rousset, R. Legros, and A. Lagrange, "Recent Progress in the Fabrication of Ceramic Negative Temperature-Coefficient Thermistors," *J. Eur. Ceram. Soc.*, **13** [3] 185–95 (1994).
[57]B. Gillot, M. Kharroubi, R. Metz, R. Legros, and A. Rousset, "Electrical-Properties of Copper and Nickel Manganite Spinels in Relation with Cationic Distribution and Thermal Histories," *Silicates Industriels*, **59** [1–2] 39–46 (1994).
[58]T. Battault, R. Legros, A. Beauger, E. Foltran, and A. Rousset, "NTC Thermistors Prepared by Chemical and Conventional Methods," *Ann. Chim.-Sci. Mater.*, **20** [7–8] 403–6 (1995).
[59]M. L. M. Sarrion and M. Morales, "Preparation and Characterization of NTC Thermistors Based on $Fe_2Mn_{1-x}Ni_xO_4$," *J. Mater. Sci.*, **30** [10] 2610–5 (1995).
[60]W. A. Groen, "Rare Earth Metal-Containing High-Temperature Thermistor"; U.S. Patent #5955937, 1997.
[61]A. Feltz, R. Kriegel, and W. Polzl, "$Sr_7Mn_4O_{15}$ Ceramics for High Temperature NTC Thermistors," *J. Mater. Sci. Lett.*, **18** [20] 1693–5 (1999).
[62]A. Feltz, "Perovskite Forming Ceramics of the System $(Sr_xLa_{1-x}Ti_{x+y}Co_yCo_{1-x-2y}O_3)$ for NTC Thermistor Applications," *J. Eur. Ceram. Soc.*, **20** [14–15] 2367–76 (2000).
[63]W. H. Bragg, "On the Structure of the Spinel Group of Crystals," *Philos. Mag.*, **31** [181–86] 88–8 (1916).
[64]W. H. Bragg, "The Structure of the Spinel Group of Crystals," *Philos. Mag.*, **30** [175–80] 305–15 (1915).
[65]S. Nishikawa, "Structure of Some Crystal of the Spinel Group," *Proc. Math. Phys. Soc. Tokyo*, **8**, 199–209 (1915).
[66]T. F. W. Barth and E. Posnjak, "Spinel Structures With and Without Variate Atom Equipoints," *Z. Kristallogr.*, **82** [5/6] 325–41 (1932).
[67]A. R. West, *Basic Solid State Chemistry*. John-Willey & Sons Ltd, Chichester, 1999.
[68]C. C. Wu and T. O. Mason, "Thermopower Measurement of Cation Distribution in Magnetite," *J. Am. Ceram. Soc.*, **64** [9] 520–2 (1981).
[69]R. Metselaar, R. E. J. Vantol, and P. Piercy, "The Electrical-Conductivity and Thermoelectric-Power of $Mn_3O_4$ at High-Temperatures," *J. Solid State Chem.*, **38** [3] 335–41 (1981).
[70]A. Feteira and D. C. Sinclair, "The Influence of Nanometric Phase Separation on the Dielectric and Magnetic Properties of $(1 - x)BaTiO_3$–$xLaYbO_3$ ($0 < x < 0.60$) Ceramics," *J. Mater. Chem.*, **19** [3] 356–9 (2009).
[71]A. Macher, K. Reichmann, O. Fruhwirth, K. Gatterer, and G. W. Herzog, "Perovskite Versus Spinel Type NTC Materials for Application at Elevated Temperatures," *Inform. Midem-J. Microelectron. Electron. Components Mater.*, **26** [2] 79–85 (1996).
[72]D. Gutierrez, O. Pena, P. Duran, and C. Moure, "Crystal Structure, Electrical Conductivity and Seebeck Coefficient of $Y(Mn,Ni)O_3$ Solid Solution," *J. Eur. Ceram. Soc.*, **22** [4] 567–72 (2002).
[73]A. Veres, J. G. Noudem, S. Fourrez, and G. Bailleul, "The Influence of Iron Substitution to Manganese on the Physical Properties of $YMnO_3$," *Solid State Sci.*, **8** [2] 137–41 (2006).
[74]J. Kulawik, D. Szwagierczak, B. Groger, and A. Skwarek, "Fabrication and Characterization of Bulk and Thick Film Perovskite NTC Thermistors," *Microelectron. Int.*, **24** [2] 14–8 (2007).
[75]X. Y. Liu, Y. Luo, and X. Q. Li, "Electrical Properties of $BaTiO_3$-Based NTC Ceramics Doped by $BaBiO_3$ and $Y_2O_3$," *J.Alloys Compd.*, **459** [1–2] 45–50 (2008).
[76]C. H. Zhao, Z. B. Wang, S. M. Wang, P. H. Yang, and C. S. Chen, "Preparation and Characterization of Negative Temperature Coefficient $(Ni,Mn)_3O_4$-$La(Mn,Ni)O_3$ Composite," *J. Electroceram.*, **20** [2] 113–7 (2008).
[77]D. Houivet, J. Bernard, and J. M. Haussonne, "High Temperature NTC Ceramic Resistors (Ambient-1000 Degrees C)," *J. Eur. Ceram. Soc.*, **24** [6] 1237–41 (2004).
[78]M. A. L. Nobre and S. Lanfredi, "Thermistor Ceramic with Negative Temperature Coefficient Based on $Zn_7Sb_2O_{12}$: An Inverse Spinel-Type Phase," *Appl. Phys. Lett.*, **81** [3] 451–3 (2002).
[79]C. C. Wang, S. A. Akbar, W. Chen, and J. R. Schorr, "High-Temperature Thermistors Based on Yttria and Calcium Zirconate," *Sens. Actuat. a-Phys.*, **58** [3] 237–43 (1997).
[80]A. Petric and H. Ling, "Electrical Conductivity and Thermal Expansion of Spinels at Elevated Temperatures," *J. Am. Ceram. Soc.*, **90** [5] 1515–20 (2007).
[81]A. Feltz, "Trends in the Development and Application of Negative Temperature Coefficient Oxide Ceramics," *Proc. Electroceram. IV*, 677–84 (1994).
[82]E. G. Larson, R. J. Arnott, and D. G. Wickham, "Preparation, Semiconduction and Low-Temperature Magnetization of System $Ni_{1-X}Mn_{2+x}O_4$," *J. Phys. Chem. Solids*, **23**, 1771–81 (1962).
[83]T. O. Mason and H. K. Bowen, "Electronic Conduction and Thermopower of Magnetite and Iron-Aluminate Spinels," *J. Am. Ceram. Soc.*, **64** [4] 237–42 (1981).
[84]T. O. Mason and H. K. Bowen, "Cation Distribution and Defect Chemistry of Iron-Aluminate Spinels," *J. Am. Ceram. Soc.*, **64** [2] 86–90 (1981).
[85]C. Metzmacher, W. A. Groen, and I. M. Reaney, "Microstructure and Electrical Properties of Mn–Ni–In Spinels," *Phy. Status Solidi a-Appl. Res.*, **181** [2] 369–86 (2000).
[86]R. Schmidt, A. Basu, and A. W. Brinkman, "Small Polaron Hopping in Spinel Manganates," *Phys. Rev. B*, **72** [11] 1–2 (2005).
[87]J. T. S. Irvine, A. Huanosta, R. Valenzuela, and A. R. West, "Electrical-Properties of Polycrystalline Nickel Zinc Ferrites," *J. Am. Ceram. Soc.*, **73** [3] 729–32 (1990).
[88]A. R. Ferreira, C. S. Furtado, and J. M. Perdigao, "Grain-Boundary and Grain Electrical Resistances in $Co_xFe_{3-X}O_4$," *J. Am. Ceram. Soc.*, **75** [6] 1708–11 (1992).
[89]S. G. Song, Z. Ling, and F. Placido, "Impedance Analysis of MnCoCuO NTC Ceramic," *Mater.Res. Bull.*, **40** [7] 1081–93 (2005).
[90]J. S. Lee, D. Y. Kim, J. Fleig, and M. Joachim, "Geometry and Electrical Properties of Grain Boundaries in Manganese Zinc Ferrite Ceramics," *J. Am. Ceram. Soc.*, **87** [10] 1895–902 (2004).

[91]S. D. Wood, B. W. Mangum, J. J. Filliben, and S. B. Tillett, "Investigation of Stability of Thermistors," *J. Res.Nat. Bureau Standards*, **83** [3] 247–63 (1978).
[92]K. M. Lawton, S. R. Patterson, and R. G. Keanini, "Direct Contact Packed Bed Thermal Gradient Attenuators: Theoretical Analysis and Experimental Observations," *Rev. Sci. Instrum.*, **74** [5] 2886–93 (2003).
[93]J. M. Zurbuchen and D. A. Case, "Aging Phenomena i Nickel-Manganese Oxide Thermistors," *Am. Inst. Phys.*, 889–95 (1982).
[94]T. Battault, R. Legros, and A. Rousset, "Aging of Iron Manganite Negative Temperature Coefficient Thermistors," *J. Mater. Res.*, **13** [5] 1238–42 (1998).
[95]P. Castelan, A. Bui, A. Loubiere, A. Rousset, R. Legros, J. Sarrias, and S. Fritsch, "Aging of Nickel Manganite Negative-Coefficient Thermistors," *Silicates Industriels*, **59** [5–6] 187–93 (1994).
[96]W. A. Groen, C. Metzmacher, P. Huppertz, and S. Schuurman, "Aging of NTC Ceramics in the System Mn–Ni–Fe–O," *J. Electroceram.*, **7** [2] 77–87 (2001).
[97]W. A. Groen, C. Metzmacher, V. Zaspalis, P. Huppertz, and S. Schuurman, "Aging of NTC Ceramics in the System Mn–Ni–Fe–O," *J. Eur. Ceram. Soc.*, **21** [10–11] 1793–6 (2001).
[98]W. A. Groen, V. Zaspalis, and S. Schuurman, "Aging of NTC Ceramics Investigated by Magnetic Measurements," *J. Mater. Sci. Lett.*, **18** [15] 1233–5 (1999).
[99]O. Shpotyuk, M. Vakiv, O. Mrooz, I. Hadzaman, J. Plewa, H. Uphoff, and H. Altenburg, "Aging Phenomena in $Cu_{0.1}Ni_{0.8}Co_{0.2}Mn_{1.9}O_4$ NTC Ceramics"; pp. 1317–20 in *Euro Ceramics VII, Key Engineering Materials, Parts 1–3*. Trans Tech Publications Inc., Zurich, 2002.
[100]P. Castelan, B. Ai, A. Loubiere, A. Rousset, and R. Legros, "Aging Study of Nickel-Copper-Manganite Negative Temperature-Coefficient Thermistors by Thermopower Measurements," *J. Appl. Phys.*, **72** [10] 4705–9 (1992).
[101]Z. B. Wang, C. H. Zhao, P. H. Yang, L. Winnubst, and C. S. Chen, "Effect of Annealing in $O_2$ or $N_2$ on the Aging of $Fe_{(0.5)}Mn_{(1.84)}Ni_{(0.66)}O_4$ NTC-Ceramics," *Solid State Ionics*, **177** [19–25] 2191–4 (2006).
[102]R. Metz, "Electrical Properties of NTC Thermistors Made of Manganite Ceramics of General Spinel Structure: $Mn_{3-x-x'}M_xN_{x'}O_4$ ($0 <= x$ plus $x' <= 1$; M and N being Ni, Co or Cu). Aging Phenomenon Study," *J. Mater. Sci.*, **35** [18] 4705–11 (2000).
[103]J. M. Varghese, A. Seema, and K. R. Dayas, "Microstructural, Electrical and Reliability Aspects of Chromium Doped Ni–Mn–Fe–O NTC Thermistor Materials," *Mater. Sci. Eng. B-Adv. Funct. Solid-State Mater.*, **149** [1] 47–52 (2008).
[104]S. Fritsch, J. Sarrias, M. Brieu, J. J. Couderc, J. L. Baudour, E. Snoeck, and A. Rousset, "Correlation Between the Structure, the Microstructure and the Electrical Properties of Nickel Manganite Negative Temperature Coefficient (NTC) Thermistors," *Solid State Ionics*, **109** [3–4] 229–37 (1998).
[105]Z. B. Wang, C. H. Zhao, P. H. Yang, A. J. A. Winnubst, and C. S. Chen, "X-Ray Diffraction and Infrared Spectra Studies of $Fe_xMn_{2.34-x}Ni_{0.66}O_4$ ($0<x<1$) NTC Ceramics," *J. Eur. Ceram. Soc.*, **26** [13] 2833–7 (2006).
[106]G.de Gyorgyfalva, A. N. Nolte, and I. M. Reaney, "Correlation Between Microstructure and Conductance in NTC Thermistors Produced from Oxide Powders," *J. Eur. Ceram. Soc.*, **19** [6–7] 857–60 (1999).
[107]M. M. Vakiv, O. I. Shpotyuk, V. O. Balitska, B. Butkiewicz, and L. I. Shpotyuka, "Ageing Behavior of Electrical Resistance in Manganite NTC Ceramics," *J. Eur. Ceram. Soc.*, **24** [6] 1243–6 (2004).
[108]K. Park, "Improvement in Electrical Stability by Addition of $SiO_2$ in $(Mn_{1.2}Ni_{0.78}Co_{0.87-x}Cu_{0.15}Si_x)O_4$ Negative Temperature Coefficient Thermistors," *Scripta Mater.*, **50** [4] 551–4 (2004).
[109]K. Park and I. H. Han, "Effect of $Cr_2O_3$ Addition on the Microstructure and Electrical Properties of Mn–Ni–Co Oxides NTC Thermistors," *J. Electroceram.*, **17** [2–4] 1069–73 (2006).
[110]K. Park and I. H. Han, "Effect of $Al_2O_3$ Addition on the Microstructure and Electrical Properties of $(Mn_{0.37}Ni_{0.3}Co_{0.33-x}Al_x)O_4$ ($0 <= x <= 0.03$) NTC Thermistors," *Mater. Sci. Eng. B-Solid State Mater. for Adv. Technol.*, **119** [1] 55–60 (2005).
[111]K. Park, S. J. Kim, J. G. Kim, and S. Nahm, "Structural and Electrical Properties of MgO-Doped $Mn_{1.4}Ni_{1.2}Co_{0.4-x}Mg_xO_4$ ($0 <= x <= 0.25$) NTC Thermistors," *J. Eur. Ceram. Soc.*, **27** [4] 2009–16 (2007).
[112]G.de Gyorgyfalva and I. M. Reaney, "Decomposition of $NiMn_2O_4$ Spine: an NTC Thermistor Material," *J. Eur. Ceram. Soc.*, **21** [10–11] 2145–8 (2001).
[113]A. Feltz and W. Polzl, "Spinel Forming Ceramics of the System $Fe_xNi_yMn_{3-x-y}O_4$ for High Temperature NTC Thermistor Applications," *J. Eur. Ceram. Soc.*, **20** [14–15] 2353–66 (2000).
[114]Y. Abe, T. Meguro, S. Oyamatsu, T. Yokoyama, and K. Komeya, "Formation Region of Monophase with Cubic Spinel-Type Oxides in Mn–Co–Ni Ternary System," *J. Mater. Sci.*, **34** [19] 4639–44 (1999).
[115]D. A. Kukuruznyak, P. Ahmet, T. Chikyow, A. Yamamoto, and F. S. Ohuchi, "Combinatorial Screening of Ternary NiO–$Mn_2O_3$–CuO Composition Spreads," *J. Appl. Phys.*, **98** [4] article no. 043710 (2005).
[116]M. Vakiv, O. Shpotyuk, O. Mrooz, and I. Hadzaman, "Controlled Thermistor Effect in the System $Cu_xNi_{1-x-y}Co_{2y}Mn_{2-y}O_4$," *J. Eur. Ceram. Soc.*, **21** [10–11] 1783–5 (2001).
[117]T. Battault, R. Legros, M. Brieu, J. J. Couderc, L. Bernard, and A. Rousset, "Correlation Between Microstructure and Ageing of Iron Manganite Thermistors," *J. Phys. III*, **7** [5] 979–92 (1997).
[118]W. M. Wang, X. C. Liu, F. Gao, and C. S. Tian, "Synthesis of Nanocrystalline $Ni_1Co_{0.2}Mn_{1.8}O_4$ Powders for NTC Thermistor by a Gel Auto-Combustion Process," *Ceram. Int.*, **33** [3] 459–62 (2007).
[119]D. A. Kukuruznyak, J. B. Miller, M. C. Gregg, and F. S. Ohuchi, "Fast Response Thin-Film Thermistor for Measurements in Ocean Waters," *Rev. Sci. Instrum.*, **76** [2] article no. 024905 (2005).
[120]M. Parlak, T. Hashemi, M. J. Hogan, and A. W. Brinkman, "Electron Beam Evaporation of Nickel Manganite Thin-Film Negative Temperature Coefficient Thermistors," *J. Mater. Sci. Lett.*, **17** [23] 1995–7 (1998).
[121]A. Basu, A. W. Brinkman, R. Schmidt, Z. Klusek, P. Kowalczyk, and P. K. Datta, "A Study of the Electronic States of $Ni_xMn_{3-x}O_{4+delta}$ Thin Films Using Scanning Tunneling Microscopy and Current Imaging Tunneling Spectroscopy," *J. Eur. Ceram. Soc.*, **24** [6] 1149–52 (2004).
[122]R. Schmidt, A. Basu, A. W. Brinkman, Z. Klusek, W. Kozlowski, S. Datta, A. Stiegelschmitt, and A. Roosen, "An Investigation into the Surface Topology and Thickness Profile of Functional Ceramic Spinel Manganate Sputtered, Evaporated and Screen-Printed Layers," *Appl. Surf. Sci.*, **252** [24] 8760–7 (2006).
[123]L. Miranda, A. Feteira, D. C. Sinclair, M. G. Hernandez, K. Boulahya, M. Hernando, A. Varela, J. M. Gonzalez-Calbet, and M. Parras, "Study of the Structural, Magnetic, and Electrical Properties of the 5H Hexagonal-Type Perovskite $BaMn_{0.2}Co_{0.8}O_{2.80}$," *Chem. Mater.*, **20** [8] 2818–28 (2008).
[124]L. Miranda, K. Boulahya, A. Varela, J. M. Gonzalez-Calbet, M. Parras, M. Hernando, M. T. Fernandez-Diaz, A. Feteira, and D. C. Sinclair, "Structure-Property Relationships of the 10H Hexagonal-Type Perovskite $BaMn_{0.4}Fe_{0.6}O_{2.73}$," *Chem. Mater.*, **19** [14] 3425–32 (2007).
[125]D. C. Sinclair, T. B. Adams, F. D. Morrison, and A. R. West, "$CaCu_3Ti_4O_{12}$: One-Step Internal Barrier Layer Capacitor," *Appl. Phys. Lett.*, **80** [12] 2153–5 (2002).
[126]T. B. Adams, D. C. Sinclair, and A. R. West, "Influence of Processing Conditions on the Electrical Properties of $CaCu_3Ti_4O_{12}$ Ceramics," *J. Am. Ceram. Soc.*, **89** [10] 3129–35 (2006).
[127]M. Li, A. Fete ira, D. C. Sinclair, and A. R. West, "Influence of Mn Doping on the Semiconducting Properties of $CaCu_3Ti_4O_{12}$ Ceramics," *Appl. Phys. Lett.*, **88** [23] article no. 232903 (2006).
[128]P. F. Bongers, "Magnetic Susceptibility Measurements of Zn–Mn Spinels." Thesis, University of Leiden, 1957.
[129]A. P. B. Sinha, N. R. Sanjana, and A. B. Biswas, "The Crystal Structure of Copper Manganite," *J. Phys. Chem.*, **62** [2] 191–4 (1958).
[130]A. P. B. Sinha, N. R. Sanjana, and A. B. Biswas, "On the Structure of Some Manganites," *Acta Crystallogr.*, **10** [6] 439–40 (1957).
[131]M. O'Keeffe, "Cation Valencies and Distributions in Spinel Structures Containing Manganese," *J. Phys. Chem. Solids*, **21** [3–4] 172–8 (1961).
[132]B. Boucher, R. Buhl, and M. Perrin, "Neutron Diffraction Crystallography of Cubic Manganite Spinel, $NiMn_2O_4$," *Acta Crystallogr. Sect. B-Struct. Crystallogr. Cryst. Chem., B*, **25**, 2326–33 (1969).
[133]V. A. M. Brabers, "Ionic Ordering and Infrared-Spectra of Some II-IV Spinels," *Phys. Status Solidi a-Appl. Res.*, **12** [2] 629–36 (1972).
[134]G. T. Bhandage and H. V. Keer, "Correlation of Physical-Properties of $Ni_xCu_{1-x}Mn_2O_4$ System," *J. Phys. C-Solid State Phys.*, **9** [7] 1325–30 (1976).
[135]V. A. M. Brabers and J. Terhell, "Electrical-Conductivity and Cation Valencies in Nickel Manganite," *Phys. Status Solidi a-Appl. Res.*, **69** [1] 325–32 (1982).
[136]V. A. M. Brabers, F. M. Vansetten, and P. S. A. Knapen, "X-Ray Photoelectron-Spectroscopy Study of the Cation Valencies in Nickel Manganite," *J. Solid State Chem.*, **49** [1] 93–8 (1983).
[137]F. Golestanifard, S. Azimi, and K. J. D. Mackenzie, "Oxygen Evolution During the Formation and Sintering of Nickel Manganese Oxide Spinels for Thermistor Applications," *J. Mater. Sci.*, **22** [8] 2847–51 (1987).
[138]M. S. Islam and C. R. A. Catlow, "Structural and Electronic-Properties of $Nimn_2o_4$," *J. Phys. Chem. Solids*, **49** [2] 119–23 (1988).
[139]C. Laberty, M. Verelst, P. Lecante, P. Alphonse, A. Mosset, and A. Rousset, "A Wide Angle X-Ray Scattering (WAXS) Study of Nonstoichiometric Nickel Manganite Spinels $NiMn_2O_3$," *J. Solid State Chem.*, **129** [2] 271–6 (1997). □